Summer 2019

Development of CASTRIP dual phase steel

Brenton Allen Hrebec

Department:

DEVELOPMENT OF CASTRIP DUAL PHASE STEEL

by

BRENTON ALLEN HREBEC

A THESIS

Presented to the Faculty of the Graduate School of the

MISSOURI UNIVERSITY OF SCIENCE AND TECHNOLOGY

In Partial Fulfillment of the Requirements for the Degree

MASTER OF SCIENCE IN METALLURGICAL ENGINEERING

2019

Approved by:

David C. Van Aken, Advisor
Ronald J. O'Malley
Michael S. Moats

ABSTRACT

Thermomechanical processing necessary to produce DP 980 steel using CASTRIP hot band was investigated. The resultant steel has an ultimate tensile strength of 1038 MPa, yield strength of 744 MPa, and total elongation of 8.6%. These mechanical properties were achieved by batch annealing the hot band at 649°C for 48 hours and cold rolling to a 20% reduction. The steel was continuously annealed to simulate a galvanization cycle with an intercritical temperature of 810°C. The possibility of improving the texture of the steel by warm rolling under dynamic strain aging conditions was investigated. Dynamic strain aging in the CASTRIP hot band was found to have an onset activation energy of 82 kJ/mol. This indicates that dynamic strain aging is controlled by carbon diffusion in ferrite. Vickers hardness and differential scanning calorimetry tests prove that warm rolling at reductions of 20% generates a higher concentration of defects than ambient temperature cold rolling. Recrystallization was not obtained during warm rolling or during the continuous annealing heat treatment. Tensile tests and x-ray diffraction results show that warm rolling in dynamic strain aging conditions does not significantly improve the texture of the steel, which remains an essentially randomly oriented texture.

ACKNOWLEDGEMENTS

I would like to thank the Nucor CASTRIP division for their financial support for this project. Nucor CASTRIP also provided the CASTRIP hot band samples for this project. Without their support, this project would not have been possible.

I would like to thank Dr. David C. Van Aken for his role as advisor. His love of learning and persistence as an investigator has helped me expand my metallurgy toolbox tremendously. I have learned many lessons from him and am very grateful for his support over the course of my graduate career. I would like to also thank Dr. Ronald J. O'Malley and Dr. Michael S. Moats for their time and effort spent on my committee, as well as for the classes they have taught and all of the hallway conversations we've had.

Dr. Eric Bohannan was a big help with his work performing X-ray Diffraction tests and Differential Scanning Calorimetry Tests. Many thanks go to Mario Buchely for his help with mechanical testing and for brainstorming ideas. Daniel Field and Viraj Athavale were great colleagues and friends. Denise Eddings, Teneke Hill, and the rest of the Materials Science and Engineering department staff were wonderful to work with.

Special thanks goes to my parents, Dennis and Ann Hrebec, and my brother Brian Hrebec, for keeping the home fires going and the home garden growing.

TABLE OF CONTENTS

Page

LIST OF ILLUSTRATIONS

LIST OF TABLES

1. INTRODUCTION

1.1. PROBLEM STATEMENT

Twin-roll, thin-strip, casting of advanced high strength steel for automotive body in white application represents a large market in the commercialization of the NUCOR CASTRIP process. The term body in white includes structural frame members used for safety such as A and B pillars that are currently produced using dual phase and press hardened steel. The goal of the CASTRIP program is to produce a dual phase microstructure that meets ASTM A1079-17 tensile standards for DP 980 steel. The tensile requirements for DP 980 steel are a minimum yield strength of 550 MPa, a tensile strength of 980 MPa, and a total elongation of 8% for a standard 50 mm gauge length.

1.2. BACKGROUND

This literature review contrasts the properties, texture, and microstructure of traditional mild automotive steel with dual phase steel.

1.2.1. Traditional Mild Steel. Beginning in the 1970s, formable mild automotive steels have been continuously cast and rolled into sheet steels. These steels can be divided into two categories based upon chemistry and processing: aluminum killed steels, and interstitial free steels [1]. Another way to classify formable steels is by their chemistry and drawability. There are four primary classifications: commercial steel, drawing steel, deep-drawing steel, and extra deep drawing steel [2]. Table 1.1 shows the yield strength, elongation, and drawability parameter (r_m) recommendations for each grade of mild steel. The distinction for each grade is seen in the elongation and

drawability parameter. Deep drawing steel can be made from either aluminum-killed steel or interstitial-free steel, while extra-deep drawing steels are exclusively made from interstitial free steel [3]. Interstitial-free steels contain extremely low amounts of soluble carbon and nitrogen compared to aluminum-killed steels. When left in solution, carbon and nitrogen have a detrimental effect on the drawability of the steel.

Table 1.1. Recommended mechanical properties for the four grades of formable mild steels. The higher the r_m value the better the drawability of the steel [2].

Steel Type	Designation	Carbon Content (wt. %)	Yield Strength (MPa)	Minimum Elongation (%)	r_m Value
Aluminum-Killed	Commercial Steel Types A, B, and C	0.02-0.15	140-275	30	1.3-1.7
	Drawing Steel Types A and B	0.02-0.08	150-240	36	1.4-1.8
	Deep Drawing Steel	<0.06	115-200	38	1.4-0.8
Interstitial-free	Extra-Deep Drawing Steel	<0.02	105-170	40	1.7-2.1

Aluminum-killed steels are steels with aluminum intentionally added during the melt practice. Aluminum is added for two purposes. The first is to deoxidize the steel by forming aluminum oxides and the second is to form aluminum nitrides (AlN) for grain size control and texture control during hot working. Table 1.2 shows a typical chemistry for aluminum killed steels.

Hot rolling for the automotive market produces a hot band coil with a sheet gauge thickness between 1.8 and 3.3 mm [4]. If the hot band is cooled quickly to below 560°C,

AlN can be kept in solid solution [5]. However, if the hot band is slowly cooled, AlN will precipitate out of solution. It is desirable to prevent precipitation of AlN during the cooling of the hot band, and instead form those precipitates during annealing of the coldworked hot band. Slowly heating steel that has AlN in solution to the annealing temperature will result in AlN clustering and precipitation on dislocation substructures and slip bands. This retards recrystallization and produces a texture with a distribution of {111} planes aligned parallel with the rolling plane (γ fiber), and thereby increases the drawability of the steel [6]. To produce galvanized sheet steel, hot band will first be pickled, cold rolled, thermally processed, and then galvanized.

Table 1.2. Typical compositional ranges (ppm) of batch annealed aluminum killed steels [6].

C	N	Al	Mn
200-500	<100 (typically 40)	200-500	1500-2000

Interstitial free steel requires vacuum degassing prior to casting. Vacuum degassing lowers the carbon and nitrogen values to 0.002-0.008 weight percent and 0.001-0.005 weight percent, respectively. Table 1.3 shows a typical compositional range for interstitial-free steels. With the addition of elements such as titanium or niobium, the remaining carbon and nitrogen can be tied up in carbides and nitrides. This leaves a ferrite matrix that is almost entirely free of carbon or nitrogen in solution. Niobium can also retard the austenite recrystallization during hot rolling, which delays the formation of

{100} planes parallel to the rolled surface that result from recrystallized parent austenite transforming to ferrite. In interstitial-free steels, deformation of the {111}<110> slip system in austenite will form a brass-type texture and subsequently transform into {111}<112> ferrite texture upon cooling where <112> designates a crystallographic direction parallel to the rolling direction and {111} designates planes parallel to the rolled surface. Thus, slowing the austenite recrystallization creates a higher ratio of {111} to {100} textures that are aligned parallel with the rolling plane. The higher the ratio of {111} planes, the higher the r_m values, which improves the drawability of the steel [7, 8].

Table 1.3. Typical compositional ranges (wt%) of interstitial-free steels [9-11].

C	Si	Mn	P	Al	N	Nb	Ti	S
0.002 - 0.008	0.01 - 0.03	0.1 - 0.34	0.01 - 0.02	0.03 - 0.07	0.001 - 0.005	0.005 - 0.04	0.01 - 0.11	0.004 - 0.01

1.2.2. Steel Drawability. Drawability is a general description of how well a material can be formed into different shapes. It is often quantified by forming cups out of sheet steel and determining the maximum depth that can be formed without defect. Cups can be round, square, or elliptical depending on the specific forming requirements [12]. Another way to represent drawability is with the Lankford parameter (r). The Lankford parameter represents the plastic anisotropy present in a sheet. This is measured as the true in-plain strain divided by the true through thickness strain of the sheet product [13]. A high r-value indicates that the sheet resists thinning, which leads to neck formation and tensile failure. This resistance to thinning is required for deep drawing and formability.

The r-value is typically measured in three different orientations in a rolled sheet. These orientations are in-plane loading at angles of 0, 45, and 90 degrees relative to the rolling direction. The r-values resulting from these three tests are commonly designated as r_0, r_{45}, and r_{90}. The average of the three r-values is represented by r_m, as shown in Equation (1).

Typical r_m values for deep-drawing steel range from 1.2 to 2, with the drawability improving as r_m increases [6]. The average Lankford parameter can be used to calculate the Limiting Drawing Ratio (LDR), which is the highest ratio of blank diameter to cup diameter that can be drawn without tearing or excessive thinning. Equation 2 shows the LDR ratio as a function of r_m and the constant n, which ranges from 0.74 to 0.79 depending on lubrication, pressure, thickness, and radius of the cup. Thus, as the r_m value increases, the limiting drawing ratio increases.

$$r_m = \frac{1}{4}(r_0 + 2r_{45} + r_{90}) \quad (1)$$

$$\text{LDR} \cong \exp\left(n\sqrt{\frac{(r_m+1)}{2}}\right) \quad (2)$$

1.2.3. Effect of Cold Rolling. Cold rolling prior to continuous annealing has been shown to significantly improve the r_m values. Cold rolling a low carbon steel (with less than 0.01 weight percent carbon) from a 60% cold reduction to a 90% cold reduction can increase r_m from 1.4 to 2 [14]. Removing carbon from solution in the steel is advantageous when engineering r_m values. Interstitial elements (particularly carbon) impedes the formation of {111} textures by promoting undesirable {100} and {110} textures, which significantly reduces the r_m values. Figure 1.1 shows the relationship between solute carbon content and r_m values at cold reductions between 50 and 95%.

Solute nitrogen also reduces the drawability of the steel, and research indicates that nitrogen should be less than 0.003 wt% for optimum drawability [15, 16].

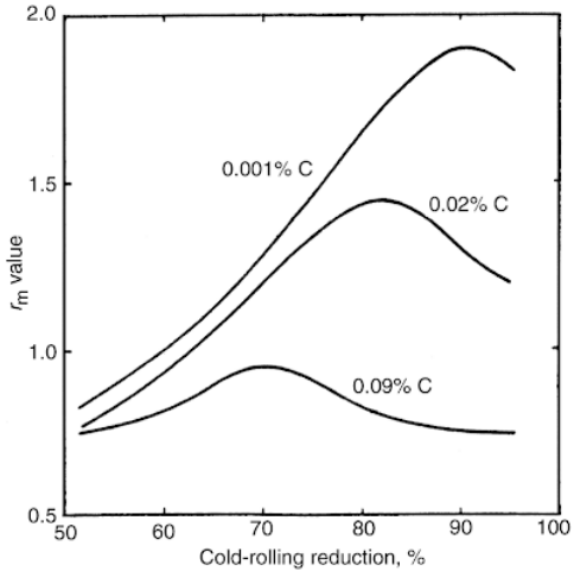

Figure 1.1. The relationship between carbon content and r_m values for cold reductions between 50 and 90% [17].

1.2.4. Processing Sheet Steel. The processing steps necessary to produce a finished coiled sheet from cast steel slabs are as follows: slab reheating, hot rolling, hot coiling, pickling, and cold rolling. Hot rolling is necessary to reduce the bulk of the material down from continuous cast thickness that typically starts at around 200 mm. This thickness is hot rolled until it is 60 to 90% thicker than the desired thickness of the finished product and coiled as hot band. The hot band is passed through a pickling station

to remove surface oxide that formed during hot rolling and subsequently cold rolled to the final thickness of the steel sheet.

Final microstructure and properties are developed during annealing of the cold rolled sheet. This may be accomplished by batch annealing, continuous annealing or galv-annealing depending upon the capabilities of the steel producer. Both interstitial-free steels and aluminum killed steels can be batch annealed or continuous annealed. However, it is most common for aluminum killed steels to be batch annealed and for interstitial-free steels to be continuous annealed, as these processing routes produce the best properties for the two types of steels. In all low carbon steels, the ferrite grain size and texture formed after hot rolling is the primary factor that controls the mechanical properties and drawability [6, 18].

1.2.5. Texture. Drawability and formability of rolled low carbon steel is significantly affected by the crystallographic texture that forms during rolling and subsequent annealing. Specific texture orientations are described by the notation of {hkl}<uvw>, which indicates that the family of {hkl} planes are parallel to the plane of the rolled sheet and the <uvw> directions are parallel to the rolling direction. Another method for representing texture is by texture fibers. These fibers describe a range of specific textures that share common directions or planes. This method of texture representation is particularly useful when describing textures influenced by cold rolling, which creates a distribution of orientations that are not accurately represented by a single {hkl}<uvw> texture intensity. Instead, the fibers represent a range of orientations that share specific directions or planes in relationship to the rolling direction and rolling plane of the sheet. Fibers are often represented in 2 or 3-dimensional Euler space, since

orientation distributions expressed with Miller indices can be mathematically converted to an equivalent Euler angle and plotted. Euler angles are three rotations that align the <100> crystal direction with the rolling direction [19]. Figure 1.2 shows a 3-dimensional plot of common fibers observed in both face centered cubic (FCC) and body centered cubic (BCC) materials using a sub-volume of Euler space.

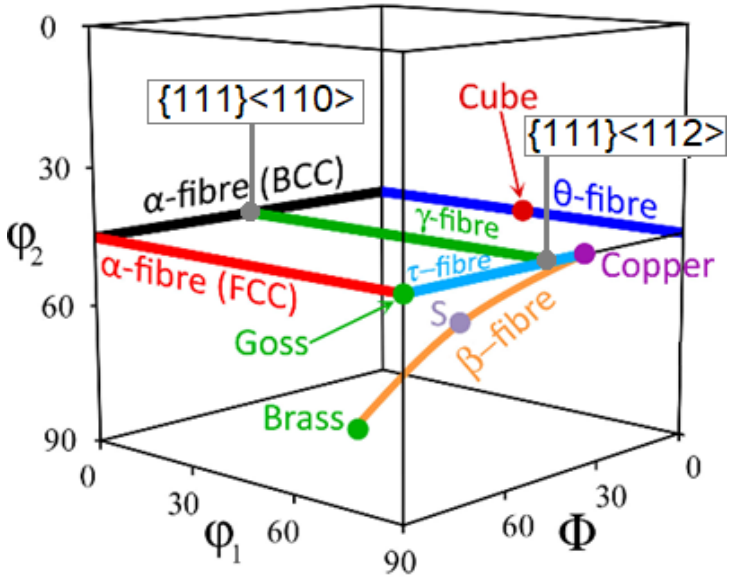

Figure 1.2. Important textures seen in both rolled and recrystallized textures in FCC and BCC materials [20]. The {111}<110> and {111}<112> orientations have been added to the graph as gray circles at the endpoints of the γ-fiber.

The two most common fiber textures that form during the thermomechanical processing of low-carbon steels are termed α and γ fibers. The α-fiber is distinguished by the <110> direction oriented parallel to the rolling direction. The specific textures that this fiber can represent are between {001}<110> and {111}<110>. In Figure 1.2, the α-

fiber runs between {100} and {110}, since it is over a 90° Euler rotation. The γ-fiber is characterized by the family of {111} planes aligning with the rolling plane of the sheet. The endpoints for the range of specific textures for the γ-fiber are {111}<110> and {111}<112>. The effect of the common texture intensities on the r_m value and the Δr (planar anisotropy) is shown in Table 1.4.

Planar anisotropy is defined as the variation between $r_{0,}$ r_{45}, and r_{90}. Equation (3) shows the calculation for planar anisotropy. Positive or negative planar anisotropy values indicate a tendency to thin at different rates relative to the rolling direction. In cup drawing this anisotropy in thinning produces a difference in cup height or ears along the circumference. Based upon the values seen in Table 1.4, the best textures for deep drawing are the {111}<110> and {111}<112> textures. These textures maximize the r_m values while keeping the Δr values at a minimum magnitude. An equal ratio of these two specific orientations is desirable to keep ear formation to a minimum, since the valleys formed every 60° during deep drawing are offset by 30° in the two different textures. Thus, the best possible texture for deep drawing steel combines the {111}<110> and {111}<112> textures in equal ratios [14, 21].

Table 1.4. r_m and Δr values for specific texture components observed in low carbon steels that have been thermomechanically processed [22].

Texture Component	r_m	Δr
{001}<110>	0.4	-0.8
{112}<110>	2.1	-2.7
{111}<110>	2.6	0
{111}<112>	2.6	0
{554}<225>	2.6	1.1
{110}<001>	5.1	8.9

Favorable γ-fiber textures are formed by cold rolling hot band steel and recrystallizing. Cold rolling, which starts with a hot band that has a randomly oriented grain structure, causes the grains to rotate to orientations that are more stable than a random (or cubic) grain orientation [23]. For example, the transformation to a favorable γ-fiber orientation from an unfavorable cubic orientation can be seen in Equation (4) [24-27]. This is a result of continued deformation. Recrystallized grains will nucleate on areas of high deformation and grow with similar orientations, which leads to a recrystallized structure of favorable γ-fiber texture. It is important to note that there is always a distribution of grain orientation, as grains will nucleate with random orientations at grain boundaries [23].

$$r_m = \frac{1}{2}(r_0 - 2r_{45} + r_{90}) \quad (3)$$

{110}<001>→{554}<225>→{111}<112>→{111}<110>→{223}<110> (4)

1.2.6. Schmid Factors. Another way to confirm the importance of the γ-fiber for the formability of the steel is through examination of the slip systems that are engaged during deformation. In BCC materials, slip occurs along the <111> directions. Slip has been shown to occur on the following planes that contain a minimum of one <111> direction: {110}, {123}, and {112} [28]. To mathematically examine slip of specific grain orientations, Schmid factors can be utilized. Equation (5) shows the equation for the Schmid factor (M). Figure 1.3 shows the angles λ and Φ in relation to the tensile axis of a specimen. Thus, a specific Schmid factor can be calculated for each specific grain orientation. In BCC materials, Schmid factors can range from 0.314 to 0.5. Schmid factor values indicate how favorably a grain is oriented for slip to occur. The higher the Schmid

factor, the more likely it is that slip will occur in the steel [28]. Figure 1.4 shows the calculated Schmid factors for some common orientations in BCC crystals. The orientations for the maximum Schmid factors correspond to orientations that result in favorable r_m values.

$$M = \text{Cos}\lambda \times \text{Cos}\Phi \text{ [28]} \quad (5)$$

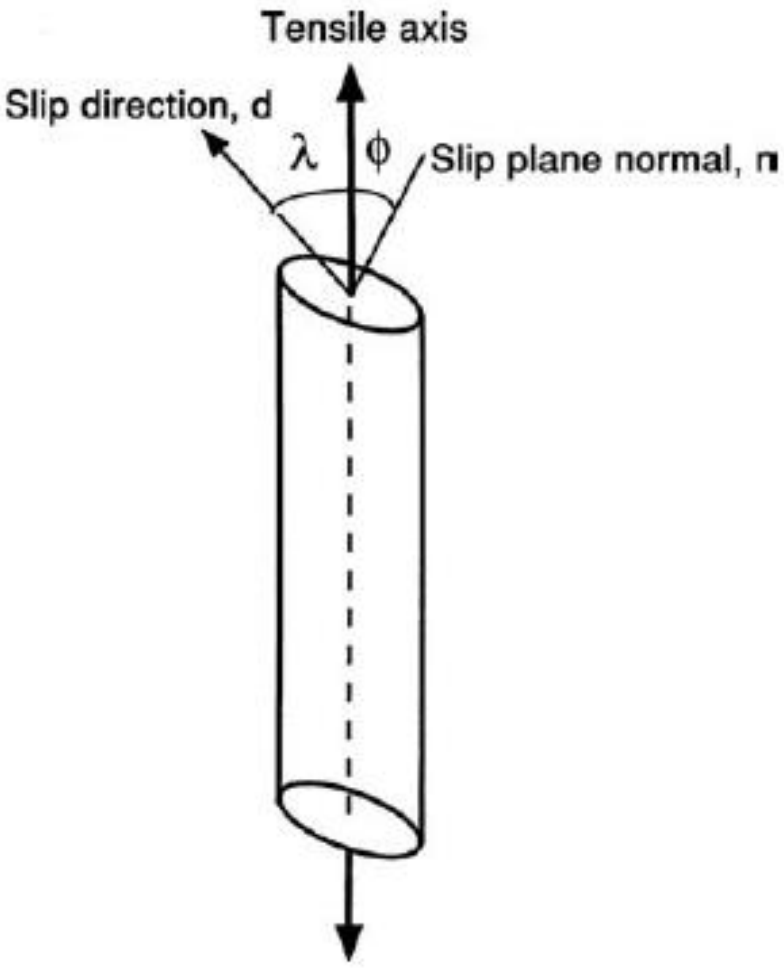

Figure 1.3. The angles defined for calculation of the Schmid factor [28].

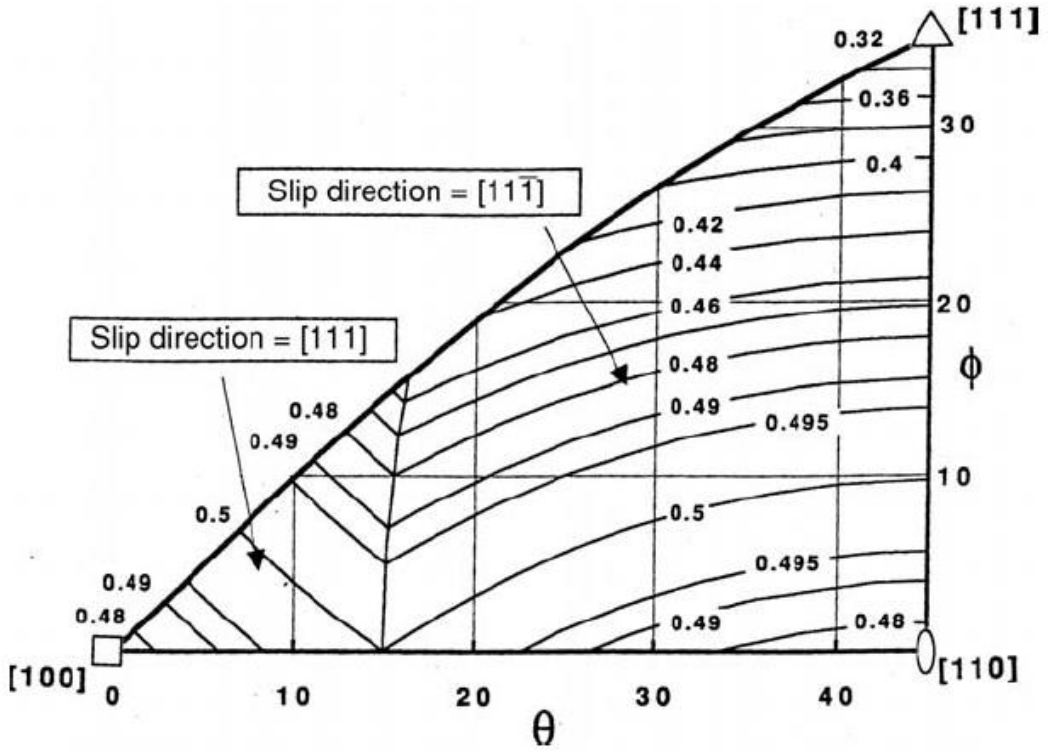

Figure 1.4. Calculated Schmid factors in BCC crystals for <111> slip. Notice that there are two different sections for two different slip directions included in the triangle [28].

1.2.7. Shear Bands. Shear bands are planar volumes that deform independent of microstructure or crystallographic orientation, and generally these slip bands form at ~35° angle to the sheet rolling plane. These shear bands are commonly observed in the Longitudinal-short plane, which allows for the angle and true thickness of the band to be measured [29]. Shear bands are necessary for nucleation of the γ-fiber. However, excessive shear bands suppress the formation of that texture. This is because heavy shear banding tends to break up grains and accommodate deformation without causing rotation of the overall matrix, i.e. high reductions reduces the nuclei for the desired texture for deep drawing. As a result, heavy shear banding decreases the γ-fiber intensity [30, 31].

Cold reductions greater than 90% will produce a loss of the γ-fiber, but maximum cold rolling to produce this loss is dependent upon steel chemistry.

For traditional aluminum killed steels that are batch annealed, a 70% reduction provides the ideal nucleation sites for development of a strong γ-fiber. For interstitial-free steels, the optimum cold reduction prior to continuous annealing can be as high as 90%. If the cold reduction is higher than this, Goss orientations will tend to nucleate on severe shear bands [34]. If the amount of cold reduction is too low, a cubic Goss texture of {110}<100> can form simultaneously with the γ-fiber [32, 33]. Both scenarios result in a reduction in r_m values. Thus, for each specific steel there is an ideal amount of cold reduction for optimum formation of shear bands and subsequent formation of the γ-fiber.

Stacking fault energy of the steel will also affect the size of the shear bands formed, since materials with a higher stacking fault energy will form larger shear bands. Larger grain sizes will also typically form a higher density of shear bands within a given grain [29]. At composition ranges characteristic of low carbon steels, carbon and aluminum additions increase the stacking fault energy, while manganese additions decrease the stacking fault energy [35, 36]. Al and Si lower the unstable stacking fault energy, which decreases the stress to nucleate dislocations in austenite. However, austenite is not typically present in significant amounts at room temperature in low carbon steels. Thus, ferrite is deformed during cold rolling low carbon steel. If the unstable stacking fault energy of the steel is low enough to initiate twinning by partial dislocation nucleation, then the shear banding will be delayed, since twinning can accommodate the deformation that would form shear bands in materials with a higher stacking fault energy [37]. This most commonly occurs in FCC metals.

Finally, if the steel is rolled in dynamic strain aging conditions above a 60% reduction, the steel can become sensitive to shear flow localization. Deformation in these conditions will cause excessive shear banding, thus decreasing texture intensity as compared to material rolled outside of the dynamic strain aging region. Excessive shear banding substitutes for grain rotation and development of the required deformation texture and subsequent {111} recrystallization structure. Dynamic strain aging is not a concern in interstitial-free steels, which does not contain solute carbon and nitrogen. In interstitial-free steels, the effect of dynamic strain aging is greatly reduced or eliminated [30, 33]. However, it is important to note that these studies show the effect of dynamic strain at reductions of 60% or greater. The effect of dynamic strain aging at lower rolling reductions has not been studied.

1.2.8. Automotive Steel. Demand for fuel efficiency in automobiles has driven significant research efforts to reduce the weight of automobiles. Steel is under constant pressure from lightweight materials, most notably aluminum, to increase strength to weight ratios to remain a competitive material in the automotive marketplace. For steel to continue to compete with aluminum for weight savings in vehicles, weight reductions of 35% or greater are required [38]. Table 1.5 shows the relationship between weight reductions and yield strength of steel in automotive applications. To achieve a 35% or greater increase in weight savings, yield strengths of 700 MPa or greater are required.

It is important to note that steel continues to be the most cost-effective solution for use in automotive applications. Since aluminum is not as strong as steel, replacing a part with the same strength is not as simple as a volume exchange of material. To meet the same strength requirements, a greater volume of aluminum must be used to replace an

equivalent steel part. Raw materials to produce aluminum cost three times as much as raw materials for steel. Production of aluminum stock is twice as expensive as the cost for producing an equivalent amount of steel. There is a 20 to 30% increase in assembly costs for aluminum parts [38-40], which stems from challenges in joining aluminum materials. Spot welding aluminum requires 2 to 3 times the welding current used for steel, and has issues with weld inconsistency, porosity and greater electrode wear [41]. To successfully join aluminum materials in automotive applications, several different techniques must be used, from fasteners and adhesives, to soldering, brazing, and welding [42]. As a result, automotive manufactures are balancing the cost of using aluminum with the weight savings gained by using a lighter material.

Table 1.5. Relationship between yield strength and weight reduction for advanced high strength steels in comparison to traditional automotive steels [43].

Yield Strength (MPa)	Weight Reduction (%)
105-275 (Mild Steel)	0
400	15-25
700	35-45
900	45-50
1100	50-55

1.2.9. Dual Phase Steel. Increasing the strength of steel allows for structural cross sections to be made thinner, which reduces the weight of the part. To this end, significant advances have been made in the steel industry to produce high strength steels that are a cost-effective solution to reduce weight in automobiles. First generation

advanced high strength steels are: transformation induced plasticity (TRIP) steels, complex phase steels, and dual phase (DP) steels [44]. Figure 1.5 shows ultimate tensile strength and elongation ranges typical of steels common to the automotive industry. DP steels are currently the most utilized first-generation advanced high strength steel. For example, the 2015 Nissan Murano contained 28% dual phase steel, in comparison to 3% of 1180 complex phase steel [45]. DP steels combine an increased work hardening rate with continuous yield behavior along with a comparatively low production cost [44, 46]. A material that exhibits continuous yielding is defined as not having a specific yield point or yield point elongation. In DP steel, this is attributed to the presence of mobile dislocations in the ferrite phase resulting from the martensite phase transformation during cooling from the intercritical annealing temperature [47].

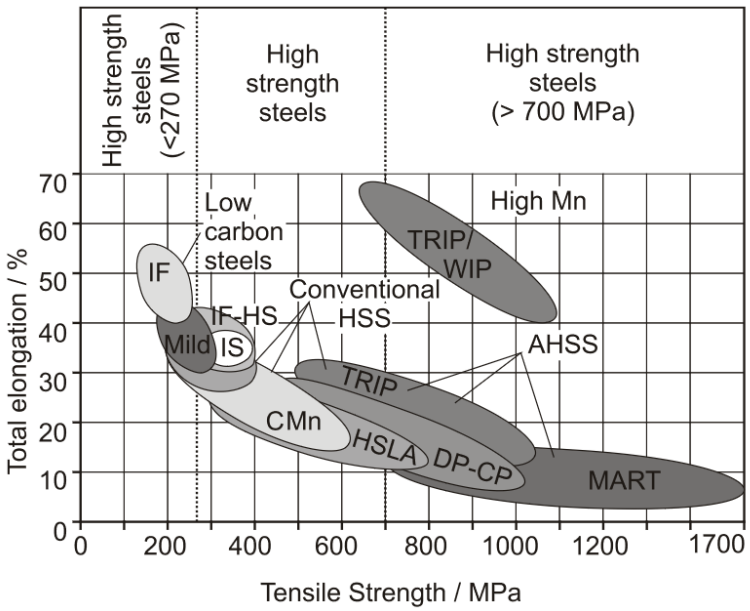

Figure 1.5. A comparison between steels common to industry. DP steels range from approximately 400 to 1180 MPa in tensile strength, corresponding to 30 to 5 percent elongation [48]

DP steels are used in several different applications throughout the automotive industry. Commercial DP steels grades range from DP 600 to DP 1180, and Figure 1.6 shows an example of dual phase steel used in a 2015 Ford Edge. DP steels are used for door beams, bumper reinforcements, roof bows, roof rails, B-pillars, A-pillars, and cross members. The combination of formability, strength, and weldability along with the wide range of available mechanical properties make these steels a very attractive choice for automotive applications. Research has been conducted using dual phase steels into panels and wheels as well, although these specific applications are not as common [49-51].

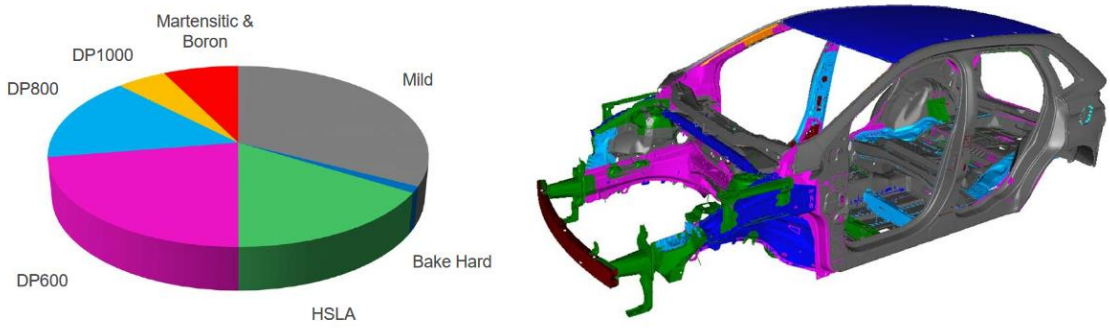

Figure 1.6. Uses of DP steel in a 2015 Ford Edge (body in white) [52]. The number in the grade of steel refers to the ultimate tensile strength of the steel, per ASTM A1079 [53].

DP steels contain significantly more alloying elements than aluminum-killed steels or interstitial-free steels, but at approximately half of the carbon content of a typical TRIP steel and this improves weldability. Table 1.6 shows a typical a chemical composition range for common grades of DP steel along with the effect of each addition

on the microstructure of the steel. There is no consensus on the best composition to obtain a specific grade. Some DP steels contain only carbon, manganese, and silicon. Others contain additional molybdenum and chromium for increasing hardenability of the steel, as well as micro-alloying elements such as niobium and vanadium for austenite grain size control [54-65]. Depending on the desired heat treatments, different combinations of austenite stabilizers, ferrite stabilizers, and micro-alloying elements may be selected. Carbon and manganese have the most significant impact on the intensity and orientation of the steel texture.

To combat the adverse effect of the solute carbon, it is recommended to bring the solute carbon out of solution in the form of carbides prior to rolling. After the rolling texture is formed, the carbon can be absorbed back into solution during intercritical heat treatment, at which point it can no longer affect the ferrite texture [57, 58]. There is one exception noted by Barnett and Kestens, who suggest that solute carbon is beneficial for increasing the {111} texture intensity. They utilized a two-step annealing process to produce an 8 μm grain size. A small grain size coupled with an 85% reduction showed an increase in {111} texture intensity for samples with high solute carbon [59].

Manganese has a more complex effect on the texture formation in steel. At very low levels (~0.02%), manganese has been shown to improve desirable γ-fiber texture intensities [60]. However, at levels above 0.4%, manganese can have a detrimental effect on the formation of the {111} rolling plane texture. Solute manganese can slow down the growth of recrystallized grains that are favorably oriented, which gives time for grains with a less favorable orientation to nucleate and grow [21]. Research shows that manganese can promote the formation of unwanted α-fibers due to carbon-manganese

dipoles that encourage strain-induced boundary conditions. Manganese can also interact with nitrogen to create an adverse similar effect [34].

Table 1.6. Composition ranges for common dual phase steel grades [54, 55].

Element	Composition Range (wt%)	Effect on Microstructure
C	0.06-0.15	Austenite stabilizer Increase martensite strength Carbides can control the austenite formation and distribution Reduces r_m values
Mn	1.5-2.5	Austenite stabilizer Solid-solution strengthener of ferrite Texture: Beneficial at 0.02%, detrimental above 0.4%
Si	<0.4	Ferrite stabilizer
Cr, Mo	<0.4	Increase hardenability (Mo - strong effect, Cr - weak effect)
V	<0.06	Austenite stabilizer Precipitation strengthener Carbide former Grain pinning in absence of Al or Nb
Nb	<0.04	Refinement of microstructure (grain pinning) Carbide former

DP steel microstructures are comprised of a ferrite matrix and a hard, secondary phase. The secondary phase is typically martensite, although ferrite-bainite steels are also classified as DP steels [61]. A martensite-ferrite DP structure is produced by heat treating at intercritical temperatures to form austenite islands and then quenching to produce the martensite islands in the ferrite matrix. There are several processing routes that can produce this microstructure. The most common method of processing is cold rolling hot

band steel to reductions between 50% and 75% and quenching after an intercritical heat treatment [62, 63]. Cold working prior to heat treatment creates additional areas in the microstructure that can act as nucleation sites for the austenite formation. Additional austenite nucleation sites are created because austenite nucleates on ferrite grain boundaries and carbides. Carbides can be located on ferrite grain boundaries or at intragranular locations [64]. Thus, cold rolling the steel is an effective method for refining the grain structure of DP steel [65]. Figure 1.7 shows typical DP microstructures after cold rolling to 56 and 69 percent reduction, heat treating in the intercritical region, and quenching to form martensite.

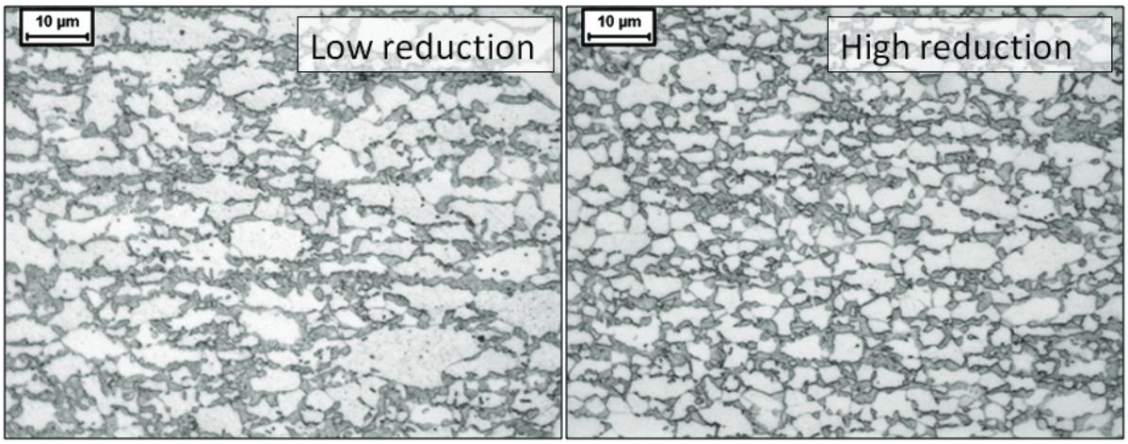

Figure 1.7. Optical micrographs of a typical DP structure. These two microstructures were produced by cold rolling at DP 800 steel to a 56 % reduction (Low reduction) or a 69% reduction (High reduction) to observe the refinement of the microstructure resulting from cold working the structure prior to heat treatment. The light phase in the micrographs is ferrite, and the dark phase is martensite [67].

Research by Chang and Preban shows that decreasing the ferrite grain size will increase the strength of the DP steel. Increasing the volume fraction of martensite will also increase the strength of DP steel. Figure 1.8 shows the effect of the mean free path in ferrite and the volume fraction of martensite on the yield strength to tensile strength ratio [68]. Research by Hwang et al., confirms the relationship between ferrite grain size and strength in DP steels [69]. Gorni and Branchini developed general equations showing the effect of the microstructure on tensile strength, yield strength, strain hardening exponent and uniform elongation of DP steel [70, 71]. Equations (6-9) show these relationships. These equations use the mean ferrite free path, which describes the average distance that a dislocation can travel in ferrite before encountering an obstacle, e.g. grain boundary or the martensite-austenite islands. In the case of DP steel, this can be defined as the ferrite grain size [68]. The ferrite grain size in the hot band can be reduced by decreasing the austenite grain size of the hot band. This is achieved by increasing the controlled cooling rate of austenite and subsequent ferrite transformation, as seen in Figure 1.9 [66].

$$YS = 203 + 855\sqrt{\frac{1}{L_{\alpha\alpha}}}\,[70] \tag{6}$$

$$TS = 266 + 548\sqrt{\frac{1}{L_{\alpha\alpha}}} + 1741\sqrt{\frac{f_\beta}{d_\beta}}\,[70] \tag{7}$$

$$\frac{d\sigma}{d\varepsilon} = 386 + 590\sqrt{\frac{1}{L_{\alpha\alpha}}} + 1722\sqrt{\frac{f_\beta}{d_\beta}}\,[71] \tag{8}$$

$$\varepsilon_{unif} = 32 - 64\sqrt{\frac{1}{L_{\alpha\alpha}}}\,[70] \tag{9}$$

Where: YS is the yield strength (MPa)
TS is the tensile strength (MPa)
$\frac{d\sigma}{d\varepsilon}$ is the strain hardening coefficient
ε_{unif} is the uniform elongation
$L_{\alpha\alpha}$ is the mean ferritic free path (μm)
d_β is the mean diameter of martensite islands (μm)
f_β is the volume fraction of martensite

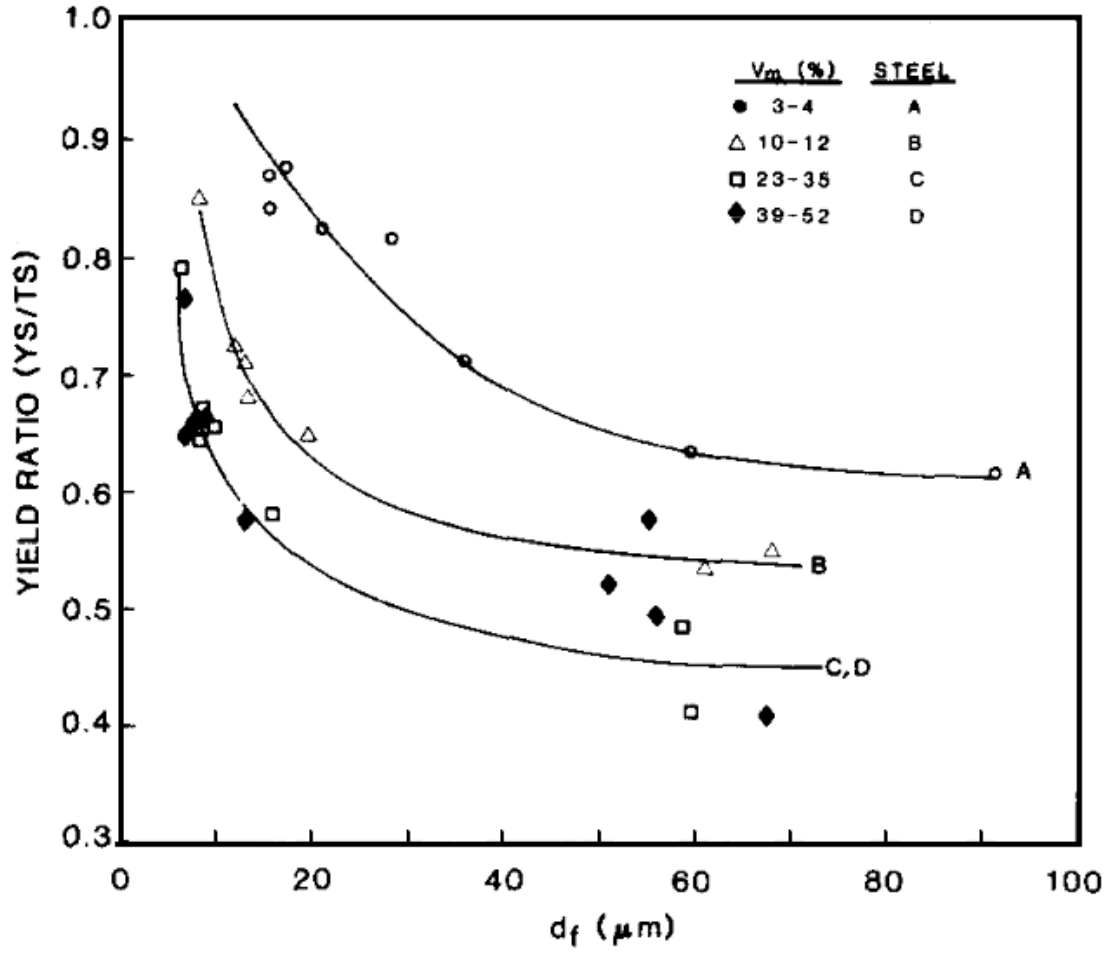

Figure 1.8. The relationship between the mean free ferritic path (ferrite grain size) and the yield strength to tensile strength ratio. As the ferrite grain size decreases, the strength of the material increases. The effect of increasing the volume fraction of martensite is also shown. As the volume fraction of martensite increases, the strength of the material increases [68].

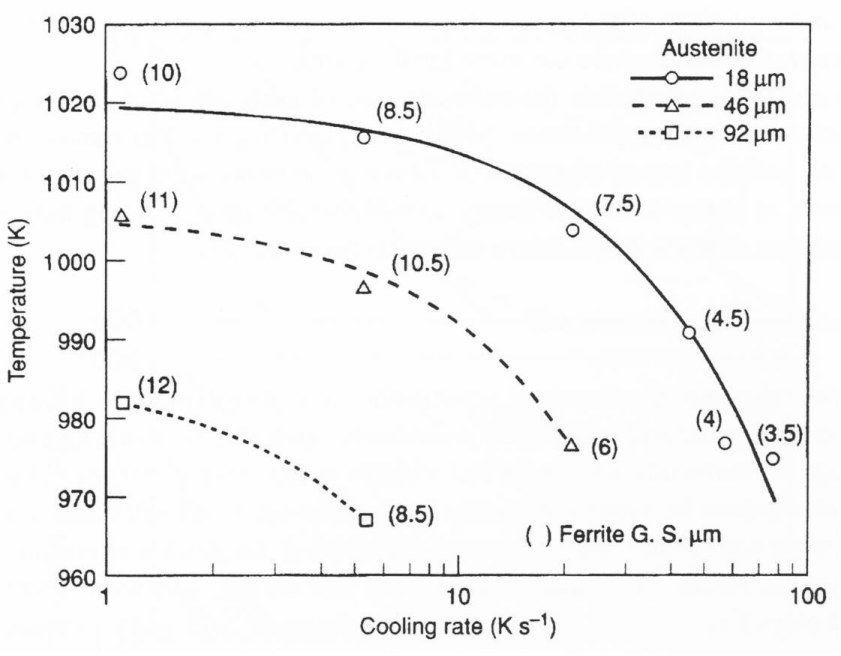

Figure 1.9. Ferrite grain size control as a function of controlled cooling rate [66]. Grain size can also be controlled by niobium or vanadium additions that act as grain pinners [54].

Two other methods of thermomechanical processing include rolling in the intercritical region or rolling in the austenite region. After rolling in the intercritical region, the steel is quenched to transform the austenite into martensite. After rolling in the austenite region, the cooling is controlled to form ferrite prior to quenching the remaining austenite to form martensite [72, 73]. Figure 1.10 shows these two thermal processing routes that are used to produce DP steel. Steel can be quenched from the intercritical region or cooled from the austenite region. The first method is similar to the thermal processing of the steel in a continuous annealing line, except the steel is quenched directly from the intercritical region instead of controlling the cooling to the temperature of the zinc bath and quenching in an air jet. The second method is commonly

used to produce DP steel by controlling the cooling of the steel after hot rolling to form ferrite grains and then quenching to form martensite from the remaining austenite [74].

Many DP steel products are heat treated in conjunction with a galvanization coating line. After pickling and cold rolling, the coil is brought to an intercritical temperature needed to grow the required percentage of austenite to meet the target mechanical properties for the steel. This heat treatment is performed in a continuous annealing line (CAL) furnace and subsequently cooled to the temperature of the zinc bath prior to dipping. Two common types of furnaces used for this application are direct fired furnaces and radiant heating tube furnaces. Direct fire furnaces can have heating rates ~40°C/sec higher than radiant tube furnaces. In both cases the furnace atmosphere is carefully controlled to prevent scale formation during the heat treatment [80].

Figure 1.11 shows the two most common thermal paths in the continuous galvanization process. In both methods the steel is heat treated in the intercritical region between the Ac1 and Ac3 temperatures. However, depending on the cooling system utilized, the steel is either: (a) quenched with water aerosol spray after the intercritical annealing to form martensite and then reheated to the zinc bath temperature, or (b) more slowly cooled to the temperature of the zinc bath and then quenched in forced air to form martensite after the zinc bath [81].

One of the most important microstructural features that needs to be carefully controlled is the volume percentage of martensite that is present in the microstructure. As the volume percentage of martensite increases, the tensile strength of the material increases linearly. Figure 1.12 shows the relationship between material strength and volume fraction martensite for a typical DP chemistry. Figure 1.13 shows the effect of the

volume fraction of martensite on uniform elongation [47]. According to Gorni and Branchini, the yield strength and uniform elongation of DP steel is a function of ferrite grain size, while the tensile strength of DP steel is a function of ferrite grain size, martensite volume fraction, and size of the martensite islands as seen in equations (7), (8) and (9) [70].

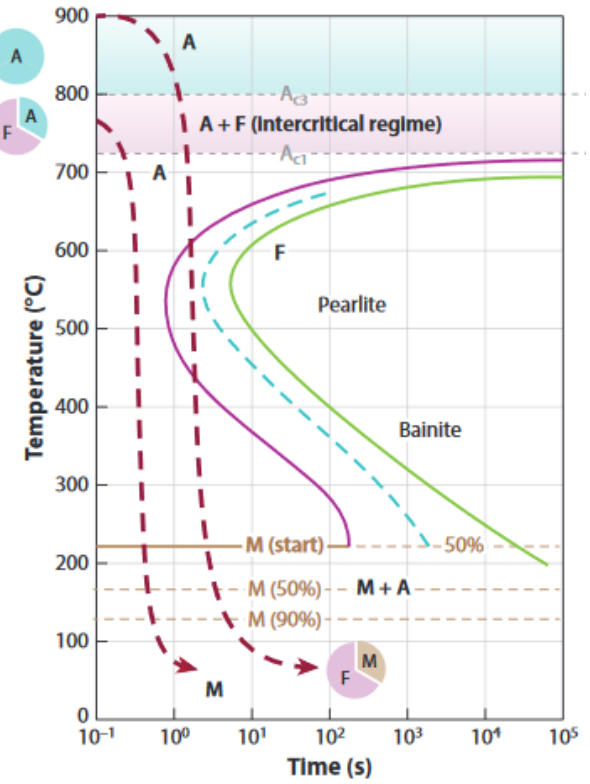

Figure 1.10. Two typical thermal cycles (red dashed lines) used to produce DP microstructures directly from rolling. The microstructures will consist of a ferrite matrix and martensite islands. The first method is rolling in the intercritical region, while growing islands of austenite and then quenching to form martensite. The second method is rolling in the austenite region and controlling the cooling to produce the desired amount of ferrite prior to quenching to form martensite [74]. If continuous annealing is performed in conjunction with galvanization, the material will be cooled from the intercritical region to the temperature of a zinc bath prior to quenching below the martensite start temperature.

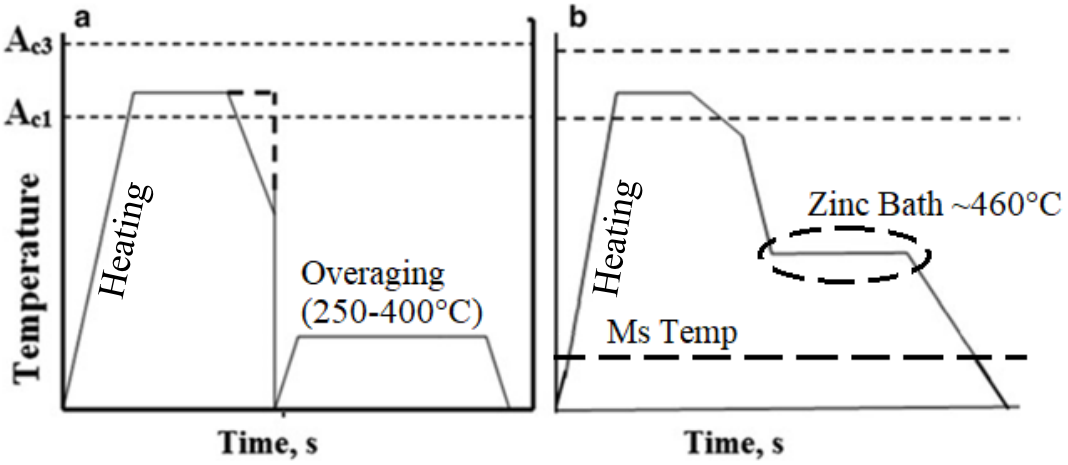

Figure 1.11. The two most common heat treatment paths used in continuous annealing. Route (a) uses a water quench and reheat system after intercritical annealing, while route (b) controls the cooling from the intercritical temperature to the zinc bath temperature, with quenching in an air jet after the zinc bath to form martensite [81]. Overaging typically occurs at ranges between 250 and 400°C in DP steels [82].

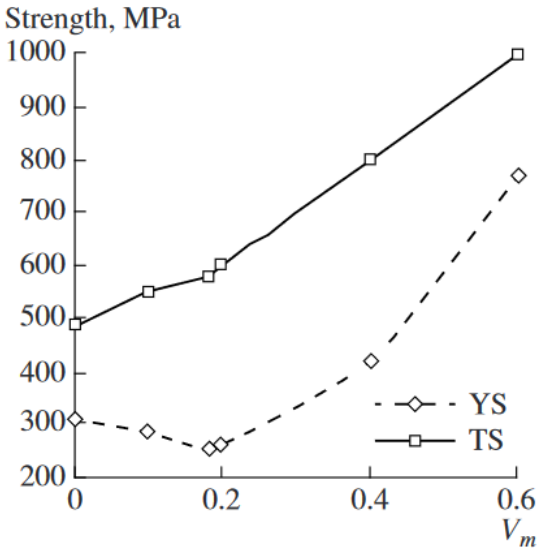

Figure 1.12. The effect of volume fraction martensite on tensile strength and yield strength for a 0.08 C, 1.6 Mn, and 0.73 Si (wt%) steel. This graph was produced by heat treating steels in a laboratory at different intercritical temperatures and quenching in water to form varying amounts of martensite. The specimens were also tempered at 200°C. In industry, quenching to form martensite typically either occurs via water spray on a run out table, or in an air jet after galvanization [47].

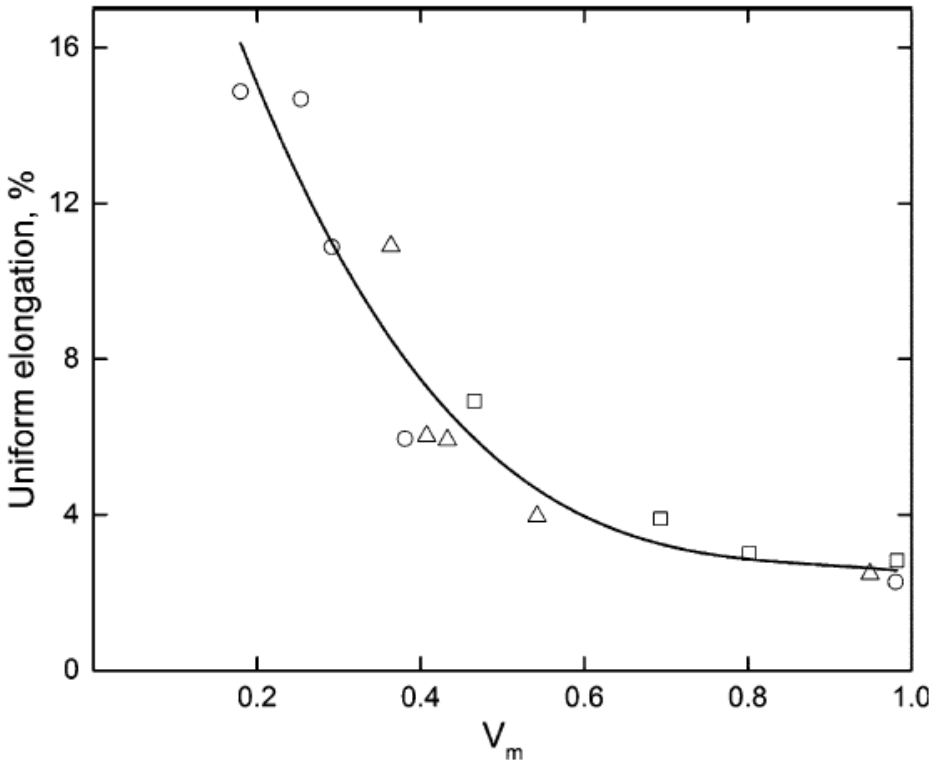

Figure 1.13. The relationship between volume fraction martensite and uniform elongation for a Cr-Mn-Si-B steel. This graph was produced by heat treating steels in a laboratory at different intercritical temperatures and quenching in water to form varying amounts of martensite. The specimens were also tempered at 200°C [54].

Martensite in DP steel can be acicular, globular, or dispersed as shown in Figure 1.14. Acicular martensite is formed by austenitizing steel with an acicular ferrite structure. Globular martensite is produced by cooling from the austenite region and holding in the isothermal region. Dispersed martensite is created by intercritical annealing cold rolled steel [75]. A primary factor in austenite morphology is the pre-existing microstructure. Depending on the nucleation sites available, austenite will either form fibrous or globular structures, as shown in Figure 1.15. If type A austenite (austenite that initially nucleates on martensite interlath positions or in a prior acicular ferrite

structure) is the primary austenite that nucleates and grows, then the microstructure will contain fibrous martensite. However, if type B austenite (globular austenite that nucleates on grain boundaries and carbides) is the dominant form of austenite growth, then the steel will have a globular martensite structure. Type A austenite is described as misorientation-rich because kernel average misorientation measurements show these grains to be qualitatively higher in internal misorientation than type B grains. This trend in local misorientation is believed to be a result of the type A austenite forming sub-grain boundaries after nucleating on acicular ferrite lath boundaries and growing together to form larger cohesive austenite grains [76]. However, these grains are closely related to the prior austenite grain structure and do not change significantly the prior austenite crystallographic texture.

The morphology of the martensite phase does not have a significant effect on the ultimate tensile strength of the dual phase steel, provided the same volume fractions of martensite are compared [75]. However, the tensile ductility, yield strength, and fracture performance is affected by the morphology of the martensite phase. A coarse and interconnected structure will show a significantly lower elongation to failure in comparison to a finer, more discrete structure [77, 78]. Decreasing the average size of the martensite islands has been shown to improve the formability of the DP steel [79].

Isothermal austenite growth is classically modeled with the Avrami equation (Equation 13). This model is also referred to as the Johnson-Mehl-Avrami-Kolmogorov (JMAK) model if homogenous nucleation is assumed [83-85]. In this form of the equation the units of the K constant are dependent upon the value of the n constant, as the units must cancel to result in a volume fraction.

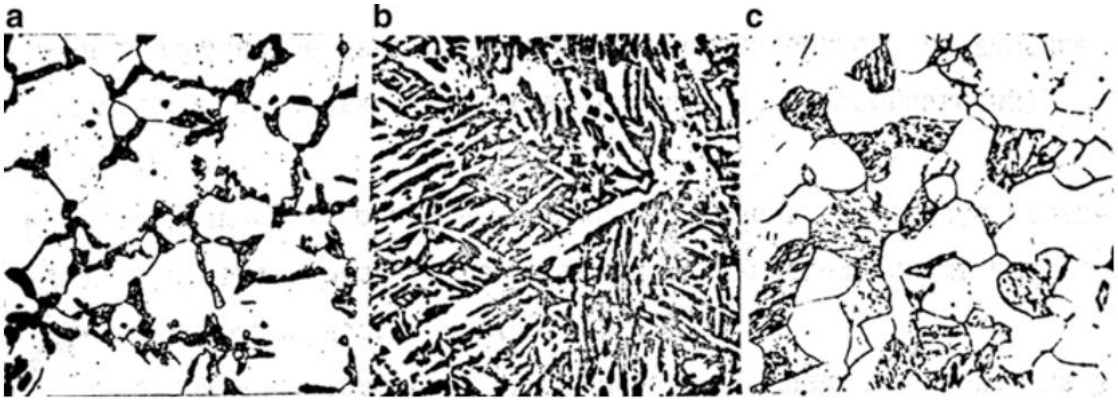

Figure 1.14. Three different types of DP microstructures resulting from different heat treatments of the same chemistry. Dispersed (a) was created by annealing and quenching a cold rolled sample. Acicular (b) was obtained by austenitizing a sample with an acicular ferrite microstructure. Globular (c) was produced by cooling from the austenite region and performing an intercritical isothermal hold [75].

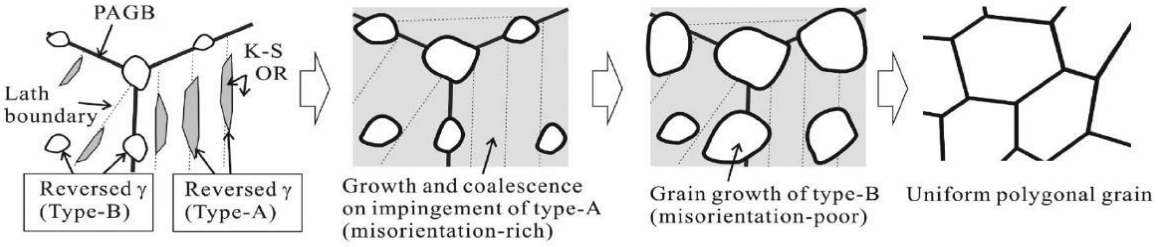

Figure 1.15. Two primary types of austenite formation that forms in martensite structures in low carbon steel [76]. Dominance of the type A austenite formation results in an acicular martensite structure upon quenching, while type B austenite creates a globular martensite structure with discrete martensite particles.

$$V_\gamma = 1 - \exp(-Kt^n) \tag{13}$$

Where:

Vγ is the volume fraction of austenite
K is a temperature-dependent rate constant $(1/s)^n$
n is an exponential term
t is time (s)

Another assumption used in this model is that given sufficient time, the microstructure will entirely transform to austenite. However, at intercritical temperatures this is not a valid assumption, because ferrite and austenite will be at equilibrium in volume fractions determined by the intercritical temperature. To account for the equilibrium between ferrite and austenite at intercritical temperatures, the austenite volume fraction term V_γ can be replaced with V_γ/V_e, the volume faction of austenite divided by the equilibrium austenite [86]. Equation (14) shows this modification to the JMAK equation. Table 1.7 shows typical Avrami parameters for intercritical annealing of a cold rolled DP steel at 770°C.

$$\frac{V_\gamma}{V_e} = 1 - \exp(-Kt^n) \text{ [86]} \quad (14)$$

Table 1.7. JMAK parameters for a ferrite-martensite steel cold rolled to 50 and 80 percent reduction and then intercritical annealed at 770°C [87]. Units for the K constant were not explicitly stated by the author.

JMAK Parameter	50% Cold Reduction	80% Cold Reduction
n	1.253	1.093
K	0.0005	0.0007

JMAK equations are appropriate for modeling austenite formation in DP steel because austenite growth is primarily controlled by carbon or manganese diffusion. Initial nucleation and growth of austenite on carbides occurs within 200 milliseconds. After the carbide and ferrite dissolution, the austenite growth is controlled by either carbon

diffusion in austenite or manganese diffusion in ferrite. Carbon diffusion in austenite controls the austenite growth at temperatures between 850°C and 950°C and reaches equilibrium in 2 to 9 seconds. Manganese diffusion in ferrite controls the austenite growth at temperatures between 740°C and 780°C and reaches equilibrium in 4 to 24 hours. True equilibrium is controlled by the diffusion of manganese in austenite, which can take between 2000 and 4000 hours to complete [88].

Specific terminology should be used to describe the different stages in diffusion controlled growth, as seen in the publications of Speer et al. and Hiller and Agren. Paraequilibrium describes the controlling condition of carbon diffusion in austenite, since it is a condition of a migrating interface between the ferrite and austenite phases. Constrained carbon equilibrium describes the state of the material after the flux of carbon atoms across the interface ceases and manganese diffusion takes over as the controlling diffusion mechanism [89, 90].

According to the research of Olivera et al., the rate of austenite formation increased with an increased heating rate to a specific temperature. In a low carbon steel heated to 800°C, increasing the heating rate from 0.1°C/sec to 1°C/sec was found to increase the amount of austenite formed from 0.5 to 0.85 volume percent. Olivera et al., attributed this to a change in controlling diffusion mechanism, and suggested that shifting the intercritical region as a result of changing the heating rate also shifts the regions of different diffusion mechanisms. At a heating rate of 0.1°C/sec, the austenite growth was considered to be controlled by the diffusion of manganese in ferrite. However, at a heating rate of 1°C/sec the controlling diffusion mechanism was considered to be the diffusion of carbon in austenite. The result of this study found a JMAK K value for a

heating rate 0.1°C/sec to be 7×10^{-5}, while a heating rate of 1°C/sec produced a K value of 2×10^{-3} [91]. The units for this K value were not specified by Olivera et al.

A study by Azizi-Alizamini et al. found that the dependence on K on heating rate is only applicable for hot rolled, low carbon steels. For a cold rolled low carbon steel, it was determined that the austenite formation kinetics were not significantly affected by the heating rate [92]. However, a different study by Mohanty et al. found that raising the heating rate of cold rolled, low carbon steel produced a higher percentage of austenite between 780°C and 820°C, which is a similar result found by Olivera et al. in their publication. Mohanty et al. also observed that a higher temperature range of 840°C to 860°C, the heating rate did not have a significant effect on the percentage of austenite formed [93]. According to Fonstein, results of heating rate experiments are very sensitive to the steel composition and the specific intercritical annealing temperature chosen. These inconsistencies could lead to different authors reaching different conclusions if there is variation in composition and temperatures in the experiments performed [94].

In a comparison between heating rates applied to low carbon steels, a heating rate of 10 K/s was found by Mohanty to produce a finer, more homogenous austenite structure than a heating rate of 50 K/s. At the higher heating rate, the recrystallization was slowed, which changed the sites of preferential austenite nucleation. A higher heating rate also causes the austenite that nucleated first to grow to a much larger size than the austenite that nucleated later in the heat treatment cycle, which results in much wider grain size distribution than observed in steel heated at a lower rate. Figure 1.16 shows a graphical representation of the effects that different heating rates have on the microstructure of a cold rolled steel [93].

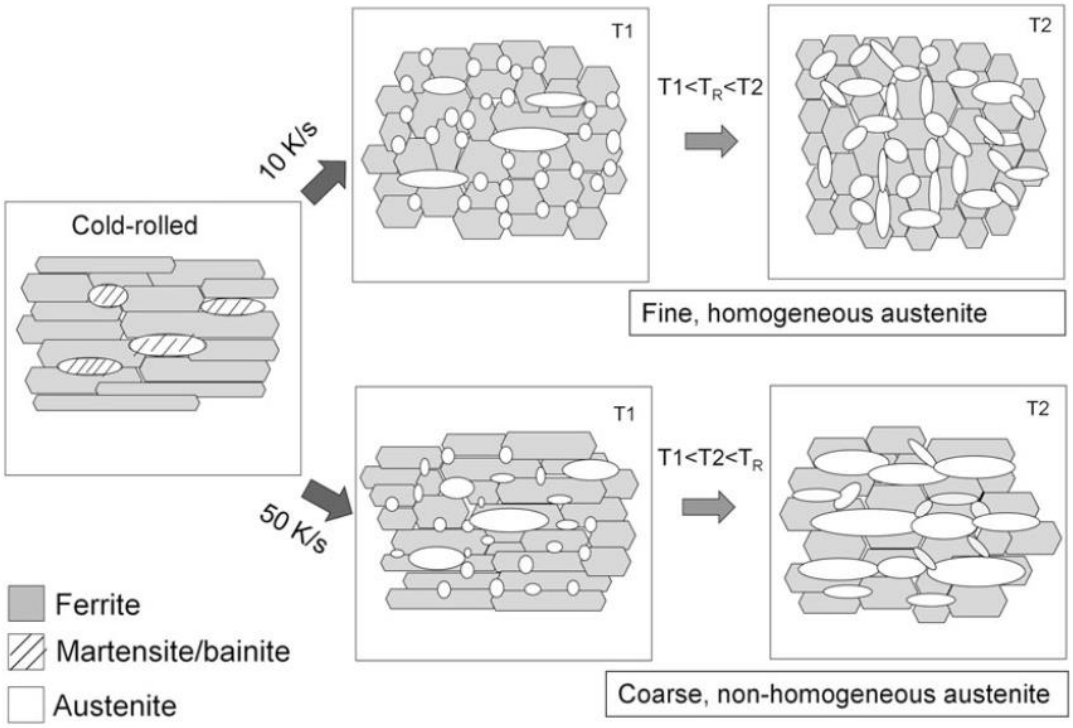

Figure 1.16. A schematic of the differences in austenite formation for two different heating rates of 10 and 50 K/s. This alters the nucleation sites for austenite formation. At a heating rate 10 K/s, the austenite forms relatively fine, homogenous austenite, while at 50 K/s, the austenite forms much coarser, non-homogenous austenite. T_r represents the recrystallization temperature, indicating that the increasing heating rate delays ferrite recrystallization [93].

1.2.10. Dynamic Strain Aging. Dynamic strain aging is manifest as serrated flow in the stress-strain curve during tensile testing. Figure 1.17 shows an example of different types of serrations that can occur during tensile testing. Serrated flow is caused by dislocation pinning by interstitial nitrogen or carbon. Solute nitrogen or carbon form Cottrell atmospheres, which is the ordering of solute atoms around dislocations. As dislocations become pinned, the remaining unpinned mobile dislocations must move faster to accommodate the applied strain rate. Increasing the speed of dislocation

movement increases the stress of the steel. The stress will increase until a dislocation line segment breaks free from the solute at a sufficiently high stress and becomes mobile. These mobile segments are typically pinned at each end and will act as a Frank-Read source and produce unpinned mobile dislocations. Increasing the density of unpinned mobile dislocations will decrease the dislocation velocity, which lowers the stress in the steel. Repeating the steps of dislocation pinning and unpinning; and thus, creation of new unpinned dislocations causes the serrations observed in a typical dynamic strain aging stress-strain curve [95].

Although dynamic strain aging is typically characterized by serrations, it is important to note that dynamic strain aging can still occur even when serrations are not seen in the stress-strain curve. This is because the serrations are a measure of the time between successive dislocation pinning, and thus at high strain rates it can be challenging to distinguish serrations [56]. In austenitic manganese steel, such as Hadfield steel, dynamic strain aging is associated with rapid work hardening.

In dual phase steels, dynamic strain aging is well documented at strain rates between 10^{-4} and 10^{-1} when deformed at temperatures between 100 and 450°C [56, 96-97]. Increasing the strain rate shifts the temperatures where dynamic strain aging occurs to a higher range of temperatures [98]. However, the temperature range is not affected by the ferrite percentage present in the dual phase steel [99]. Dynamic strain aging occurs as a result of dislocation interaction with either solute carbon or nitrogen in dual phase steels. Warm rolling in dynamic strain aging conditions is typically avoided, since it can cause heavy shear banding that decreases the texture intensity. This heavy shear banding is similar to undesirable shear banding resulting from excessive cold rolling on texture

intensities, as discussed in section 1.2.7. The effect of dynamic strain aging on texture at lower reductions (below 60%) has not been studied.

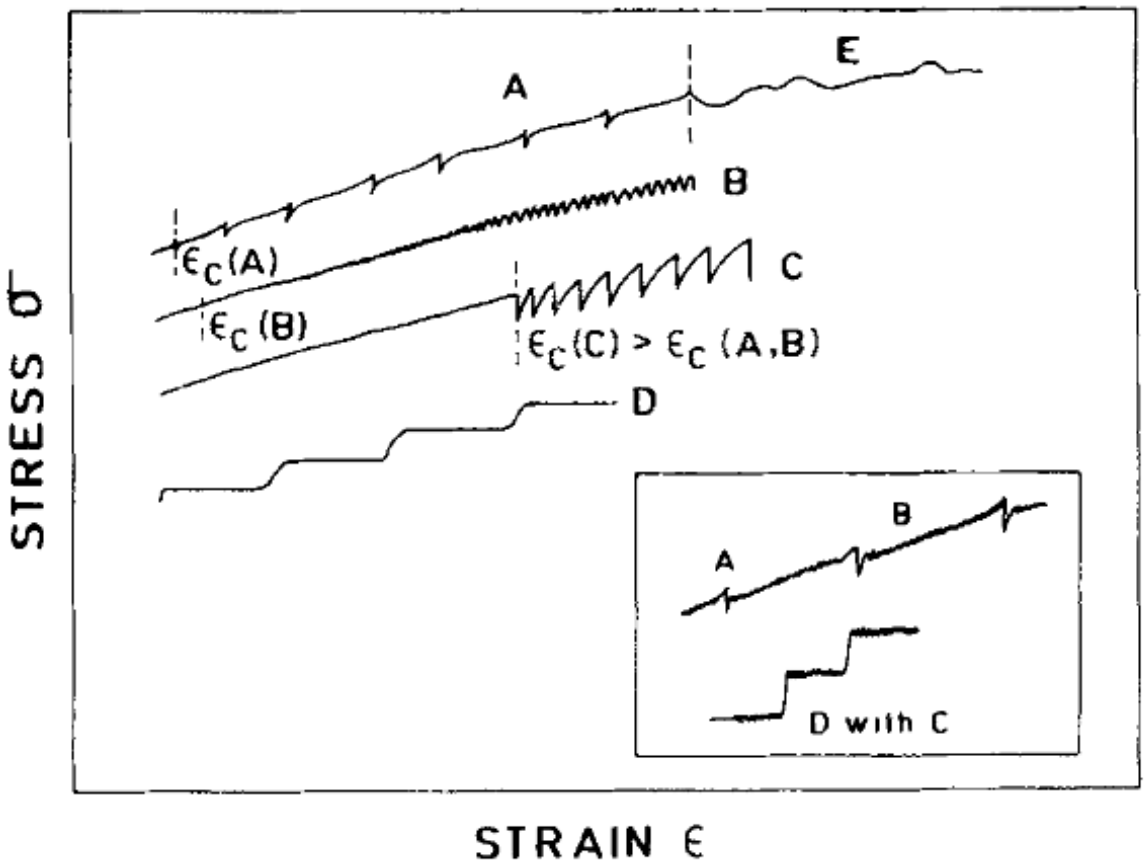

Figure 1.17. Types of serrations observed in steels. Type A serrations occur at lower temperatures and lower strain rates. Type A serrations are associated with deformation bands that have started at the same place and have propagated uniformly through the steel. Type B serrations are related to Type A mechanisms that are deformed at a higher strain rate. Type C serrations are associated with high temperatures and low strain rates. The mechanism for Type C serrations is dislocation unlocking, which results in a periodic decrease from the average stress. Type D serrations result from high temperature pre-straining prior to significant deformation. The serrations are driven by band propagation, (not accompanied by work hardening and thus no strain gradient) at the band front as it moves through the material [100].

1.2.11. The Castrip ® Process. Approximately half of the steel produced in the world is flat steel product. Of the flat steel produced, a large portion is in the form of steel coils. Steel coils are used in many applications, most notably the automotive industry, which accounts for 12% of the overall global steel consumption [38, 101]. Prior to 1989, steel coils were produced from continuous cast slabs. A typical minimum thickness for a continuous cast slab used for sheet steel production is 200 millimeters. To produce sheet steel from these slabs, 6 to 9 hot rolling mill stands in addition to a pickling station are required to produce a hot band coil. In 1989, a new thin-slab casting technology was introduced to produce slabs ranging from 50 to 70mm in thickness. Thin-slab castings are capable of directly rolling strips from the initial casting, which eliminate the need for roughing steps in the process. This significantly reduces the energy and cost in producing thin gauge sheet strips. However, significant hot rolling of thin strip products is still required to produce sheet product [102-104].

The Castrip® Process is the next technological step in producing thin sheet steel products. A simplified diagram of a typical CASTRIP line is shown in Figure 1.18. The length of the line from caster to coiler is 60 meters, while a typical slab caster is between 500 and 800 meters in length. Research shows that direct strip casting can reduce plant energy consumption by 90% and greenhouse gas emissions by 80% in comparison to traditional continuous casting technology [105, 106]. The economic benefit of the CASTRIP process is a direct result of the reduced plant footprint, as the typical roughing and hot rolling steps are not necessary for CASTRIP production. Instead of 6 to 9 rolling stands used in continuous casting, CASTRIP utilizes one or two hot rolling stands, after which the steel is directly cooled and coiled [107].

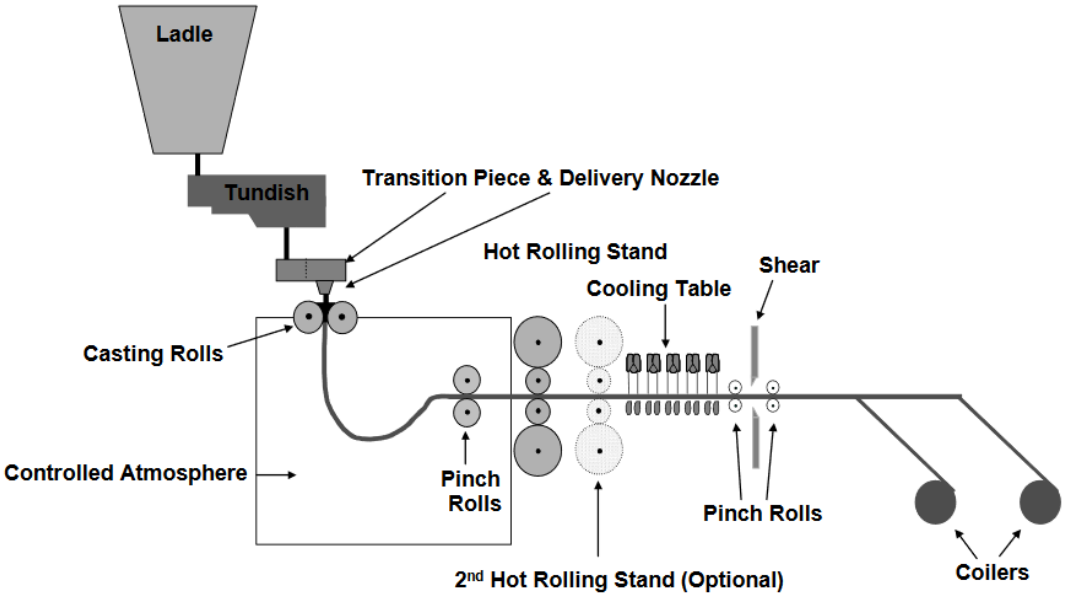

Figure 1.18. A simplified diagram of the components in a typical CASTRIP process. The distance from ladle to coil is approximately 60 meters [107].

CASTRIP technology utilizes a twin-roll casting mechanism, which is a concept that was first conceived by Sir Henry Bessemer in 1857. Twin roll casting, however, was not feasible until the modern understanding of steel solidification and implementation of modern computer controls [105]. CASTRIP research and development began in 1989, when Nucor Steel (United States of America), BlueScope Steel (Australia), and IHI (Japan) formed a conglomerate to pursue twin-roll casting technology. In the mid-1990s, CASTRIP began focusing on low carbon steels as a viable product for steel strip production. There are currently two Nucor CASTRIP facilities in the United States, located in Blytheville, Arkansas and Crawfordville, Indiana. Both plants produce low-

carbon sheet steel between 1.5 and 2 mm thick that is commercially sold for use in applications such as furniture, shelving, and roofing [108-110].

In the steel casting industry, the use of a twin-roll solidification system is unique to the CASTRIP process, although the aluminum industry has utilized twin-roll casters since 1954 [102, 111]. Figure 1.19 shows a simplified schematic of the twin rolls used in the CASTRIP process. To achieve cost-effective casting using the twin roll design, extensive research has been done in the following areas: 1) delivery and distribution of molten metal to the rolls, 2) containment for the melt on the roll edges, 3) solidification mechanisms and parameters, and 4) deflection of rolls due to thermal gradients and mechanical loading. All of these factors influence strip quality and centerline porosity which are common problems in twin-roll castings [105, 107, 112].

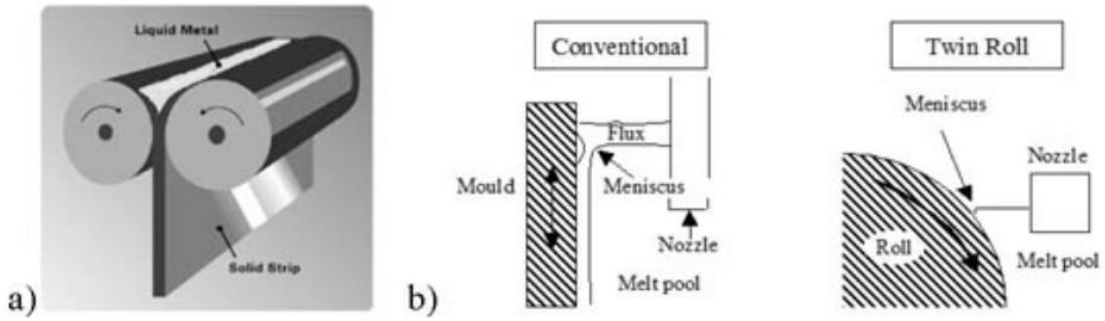

Figure 1.19. A simplified schematic of a typical twin-roll used in the CASTRIP process (a), shown in comparison to a conventional continuous casting mold (b) [110].

Solidification of the strip is one of the key challenges of the CASTRIP process. A typical total solidification time in the CASTRIP process is between 100 and 200

milliseconds. In comparison, the total solidification time for a continuous caster is several orders of magnitude greater. Because the solidification time for CASTRIP products occurs so quickly, controlling the casting process is much more challenging than conventional casting methods. The solidification path that the steel takes is an important factor that must be adjusted to produce a sound final product. Solidification through the peritectic region will result in a volume change of approximately 0.3% that can potentially overstress the shell formed early in solidification, which means that the delta ferrite to austenite transformation must be engineered to occur when the shell is thick enough to withstand the stress caused by the volume change. If this is not accomplished, cracking originating on the surface of the cast sheet may occur.

One of the most important factors in the CASTRIP process is the heat flux between the twin-rolls and the steel melt. In continuous casting, mold powder is used to control the heat transfer between the mold and the molten steel. However, in twin roll casting, there is no mold powder used. As a result, the heat transfer between the rolls and the molten steel is controlled by the direct contact of the molten steel with the water cooled, copper rolls. The surface roughness of the rolls is a very important variable in the CASTRIP process, as it directly affects the heat transfer coefficient between the rolls and the steel melt. A good understanding of the surface wetting behavior of the steel melt is necessary, as this will also affect the heat transfer and consequently the solidification rate [110].

The casting speed of the strip is another major factor in the heat flux between the steel shell and the roll. The heat flux is inversely related to the strip speed. Consequently, the thickness of the strip will increase or decrease as the strip speed changes. Figure 1.20

shows the heat flux in relation to radial distance from the beginning of the solidified shell (position 1) to where the shell exits the roll (position 6). For a low casting speed of 4m/min, the strip had a thickness between 6 and 7.5mm, while a high casting speed of 7 to 8 m/min produced a strip thickness of 4mm [113]. At high strip speeds, the heat flux will follow a quartic trend in relation to the radial distance along the solidification roll, while a slow strip speed follows a bell curve trend. The valley in the high-speed casting heat flux (Figure 1.20) is caused by liftoff of the strip from the rolls between positions 3 and 4 as the shell shrinks away from the roll. This does not occur in the low strip speed conditions because the shell is 2 to 3 mm thicker, which allows for contact to be maintained between the solidifying sheet and the rolls [114].

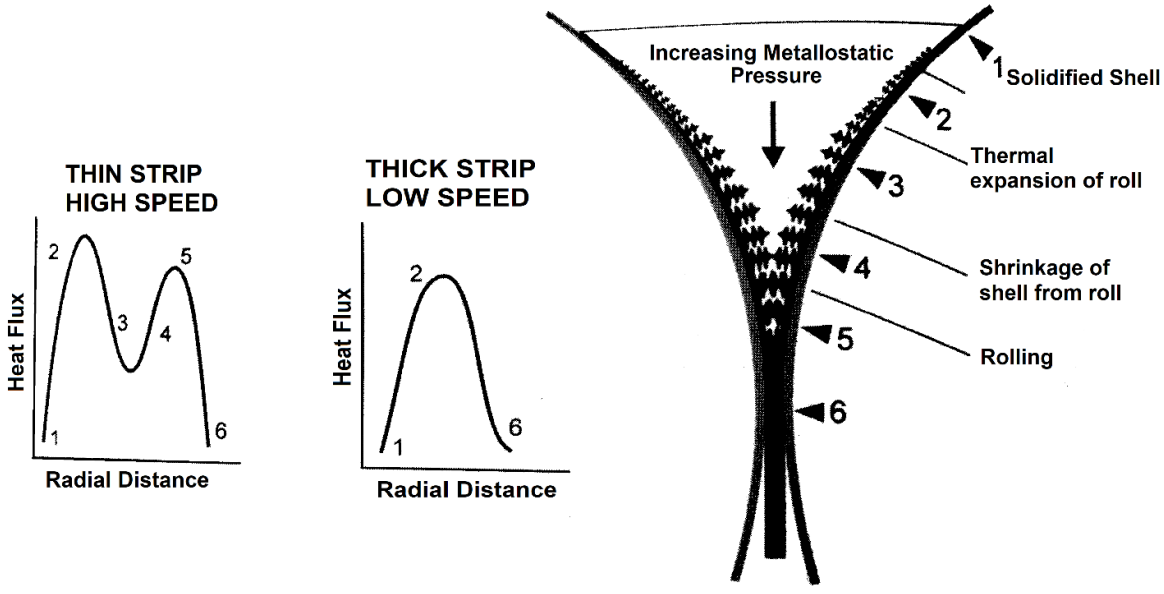

Figure 1.20. The heat flux at a high (7 to 8 m/min) and low (4 m/min) strip speed at six different locations along the roll surface [114].

The high rate of heat extraction results in a fine dendrite structure in the solidified strip. Figure 1.21.a shows a typical as-cast structure formed during the CASTRIP process. This microstructure is very different compared to a typical continuous cast structure that is shown in Figure 1.21.b. A distinct columnar dendrite structure is observed where the two shells of the steel strip have grown together. This stands in contrast to the four walls of a typical continuous casting that typically transitions to an equiaxed structure. If the heat flux is not equal for both sides of the shell, the centerline will shift from the middle of the strip towards the side with less heat extraction.

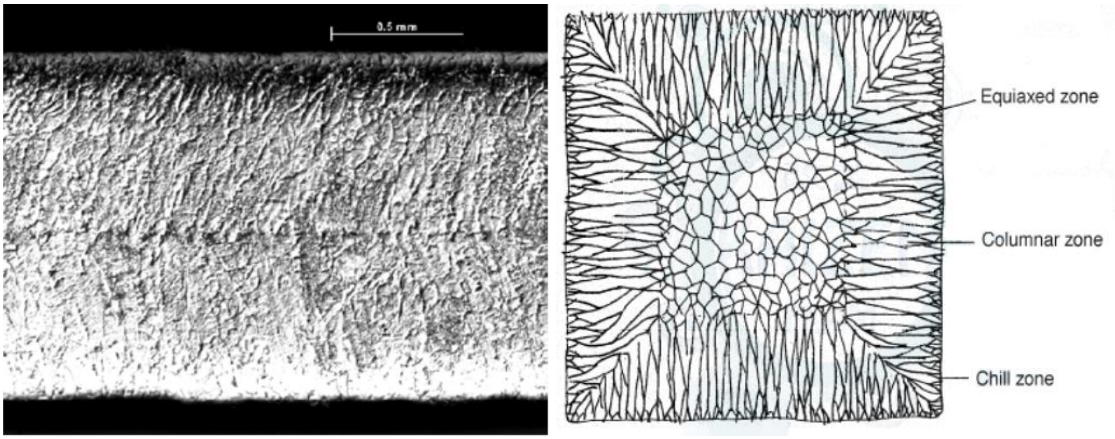

(a) (b)

Figure 1.21. The dendrite structure of an as-cast low carbon steel strip produced via the CASTRIP process (a) [115], and a typical continuous cast structure (b) [113]. In a typical twin-roll strip, the dendrite structure is fine and directional, with no equiaxed zone. The centerline of the strip can be clearly seen where the dendrite structure meets in the middle of the strip, leaving shrinkage porosity.

Research shows that typical r_m values for CASTRIP low carbon grades are approximately 1 [116]. Steels with r_m values of 1 have a crystal structure that is almost

entirely randomly oriented [117]. The solidification texture of the hot band should contain a {001} component parallel to the rolling plane. A cubic texture component could cause the r_m values of 0.93 and 0.96 reported for a specific grade of CASTRIP steel [116]. In contrast, deep drawing steels can reach r_m values as high as 2.1 [2]. This shows there is still much room for improvement in the texture of CASTRIP low carbon steel. In conventional steel making this is accomplished with reductions of 70% or more. However, the CASTRIP process is limited to cold reductions of 20% or lower. Thus, to produce CASTRIP products with a desirable texture, alternative methods to improve the texture must be pursued.

1.3. RESEARCH GOALS

The following research will explore possible dual phase microstructures, mechanical properties, and textures that can be achieved by thermomechanically processing CASTRIP as-rolled low carbon steel. Isothermal heat treatments have been performed and a typical continuous annealing line thermal cycle has been simulated. The mechanical properties and microstructures of the resultant DP steel will be compared to the equations of Gorni and Branchini. CASTRIP is limited to a 20% cold reduction, which is insufficient to provide nucleation sites for forming discrete martensite islands. To provide additional nucleation sites, alternate thermomechanical processes have been studied, such as growing carbides through batch annealing and warm rolling in dynamic strain aging conditions. The effect of the thermomechanical processing on the texture of the material is explored.

2. EXPERIMENTAL PROCEDURES

Phase equilibrium calculations were performed using the Equilib module in FactSage 7.1 using the FSstel database. Table 2.1 shows the chemical composition of the hot band steel obtained from CASTRIP. The percent of the BCC and FCC phase was calculated and graphed by raising the temperature between 650 and 825°C and raising the temperature in increments of 25°C. The possible carbide formation was also calculated from the same chemistry. The chemistry of the last 15% liquid to solidify was calculated and the possible carbide formation was determined and graphed.

Table 2.1. Chemical composition provided by CASTRIP utilized for FactSage Equilib analysis to determine the intercritical region of the steel in equilibrium conditions.

C	Mn	Cr	Ni	Si	Mo	Cu	V	P	N
0.07	2.23	0.89	0.05	0.44	0.36	0.1	0.007	0.015	0.004

Critical temperatures were experimentally measured using a resistivity method as described by Harrington [118]. A room temperature sample was placed in a tube furnace at 900°C under an argon gas atmosphere to determine the austenite start (Ac_1) and finish temperature (Ac_3). The heating rate was 16°C/sec. The temperature was continuously measured with a K-type thermocouple welded to the sample. The voltage change across the material was measured following a procedure reported by Harrington [118]. There are two competing factors that affect the resistivity of the material. As the temperature of the material increases, the voltage across the material will increase. As the steel transforms

from a BCC to an FCC structure in the intercritical region the resistivity of the material will change. Thus, to discern the interaction of these two effects, the slope of both the temperature data and the voltage data was carefully examined to determine the best correlation to the phase transformation.

A Stanat TA 315 laboratory rolling mill, equipped with a 4-high rolling configuration, was utilized to roll the sheet steel. The rolling mill contains load cells that records the loading during rolling. Percent reduction was determined by measuring the steel thickness with a digital caliper after each rolling step. Rolling was conducted at room temperature and at an elevated temperature of approximately 500°C to induce dynamic strain aging conditions. For elevated temperatures, the steel was heated in a nearby furnace approximately 10°C above the target rolling temperature. This compensated for heat loss during transfer from the furnace to the rolls.

Isothermal heat treatments for 30 minutes at a 700, 725, 775, and 800°C were conducted in a Sentry molten salt pot furnace and subsequently quenched in water. Prior to heat treatment, the as-received CASTRIP steel was cold rolled to a 20% and 65% reduction. The temperature of the molten salt bath was confirmed by welding a type-K thermocouple to samples of interest, in addition to the furnace thermocouples used for temperature control.

A 48-hour subcritical heat treatment at 649°C was performed on the as-received CASTRIP steel to coarsen carbides within the microstructure prior to rolling. Steel samples were placed in sealed stainless-steel bags along with graphite and machining chips to minimize decarburization. After the completion of the 48-hour treatment, the

stainless-steel bags were removed from the furnace and air-cooled. After cooling was complete, the steel was subsequently cold rolled.

An industrial galvanization cycle was simulated using two Sentry molten salt pots with one set to an intercritical temperature and one set to a low temperature simulating zinc galvanization. The heating rate of the sample was controlled by placing the sample between two metal plates during heating. The heating rate was held constant throughout each experiment at ~14.6°C/sec. The samples were heated to an intercritical temperature of 760°C or 810°C and held for 24 seconds at that temperature. After the intercritical heat treatment, the samples were air-cooled to 425°C and placed in the low temperature molten salt furnace. The salt bath was set to 425°C, which the temperature of a typical zinc plating bath. After holding at 425°C for 20 seconds, the sample was fan-cooled. This simulated the cooling rate typical for air jet cooling of a steel strip after zinc plating bath. Temperatures were monitored with a K-type thermocouple welded to the sample. Figure 2.1 shows the final thermal cycle used for the galvanization simulation as compared to a typical galvanization thermal cycle reported by CASTRIP. The final galvanization simulations will be referred to hereafter as continuous annealing at either 760°C or 810°C, indicating the intercritical temperature of the galvanization simulation.

Samples for metallography were mounted on-edge, in Bakelite, with the short-longitudinal being the plane of polish. Standard metallographic procedures were employed to incrementally grind and polish. The final polishing utilized 0.05 μm colloidal silica. 2% Nital was used to etch the samples prior to optical microscopy. ImageJ software was used to quantify the volume fraction of martensite and the grain size of each phase. Three total measurements were taken for the volume fraction statistics.

Two hundred total measurements were taken for grain size statistics, with two measurements per grain of the shortest and longest distance for each grain.

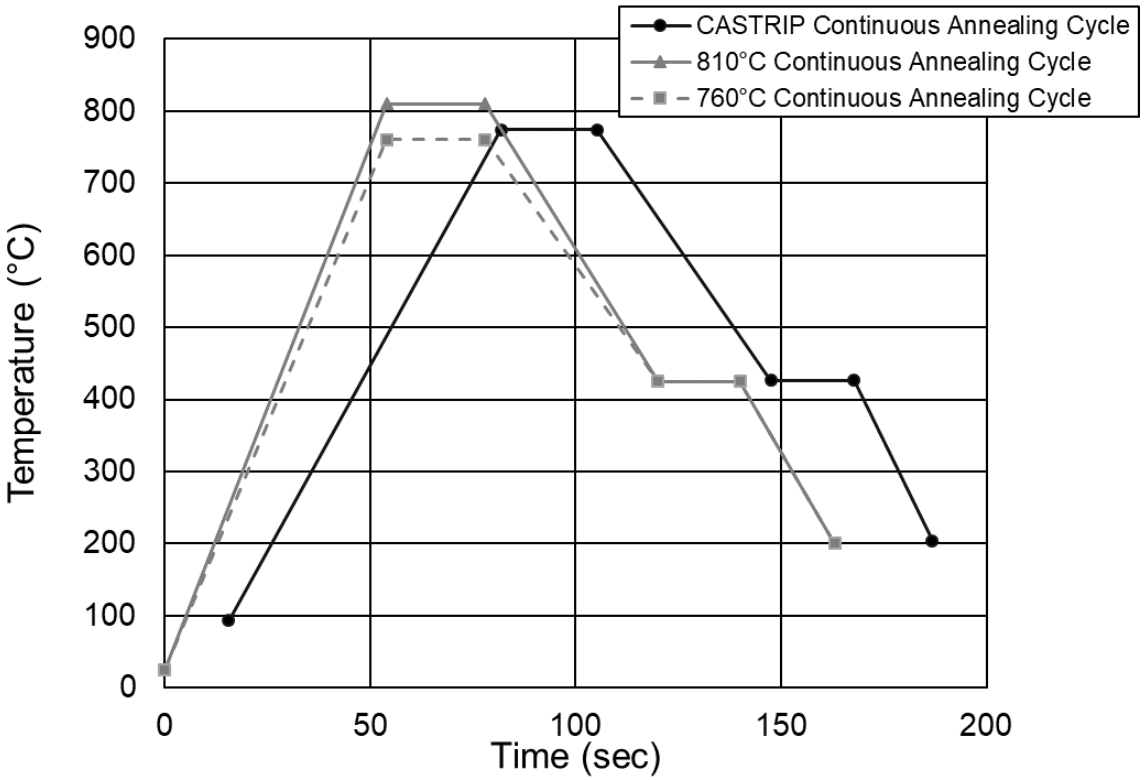

Figure 2.1. Galvanization simulation cycle applied to CASTRIP steel. A typical thermal cycle provided by CASTRIP is shown for comparison. The heating rate was slowed by placing the sample between 2 plates of steel prior to submersion in the molten salt bath. The samples were air-cooled between the intercritical temperature and the simulated zinc bath temperature. Fan-cooling was performed to simulate air-jet cooling rates typically used in industry.

Tensile testing of the material was performed using full size sheet tensile specimens that were prepared according to ASTM E8. The specimens were pulled at a strain rate of 0.005 mm/sec, and the strain was measured with a laser extensometer. Each

value reported is an average of three tests. Rockwell C hardness measurements were taken in accordance with ASTM E18. Vickers hardness was performed with a Struers Duramin hardness tester using 4.91 N of force for 10 seconds.

Dynamic strain aging tensile tests at elevated temperatures between 100 and 510°C were performed. Strain rates between 0.00002 and 0.1 s^{-1} were tested. The strain rate was calculated by dividing the gauge length of the tensile sample (50 mm) by the displacement rate of the tensile test. The resulting data was compiled into an Arrhenius plot.

X-ray diffraction (XRD) measurements were conducted using a PANalytical X'Pert MPD diffractometer system. The rolling direction of the material was recorded to determine the relationship between the rolling direction and the texture formation. Specific 2 theta angles were chosen to measure the {110} and {200} pole figures. Each sample was scanned through a 90° tilt and a 360° rotation to create a pole figure for the chosen 2 theta angle. See Figure 2.2 for a graphical explanation of the angles scanned in relation to the rolling direction. These texture measurements were used to compare the texture between the as-received CASTRIP steel and CASTRIP steel that was batch annealed, warm rolled, and continuously annealed.

Prior to testing, the as-received CASTRIP steel was batch annealed and either cold or warm rolled at 500°C to a 20% reduction. DSC measurements were conducted using a TA Q600 system. The system was operated under flowing argon gas during the entire procedure. The samples were slowly heated to 700°C, cooled to 35°C, and reheated to 700°C. Heat flow and mass of the sample was recorded.

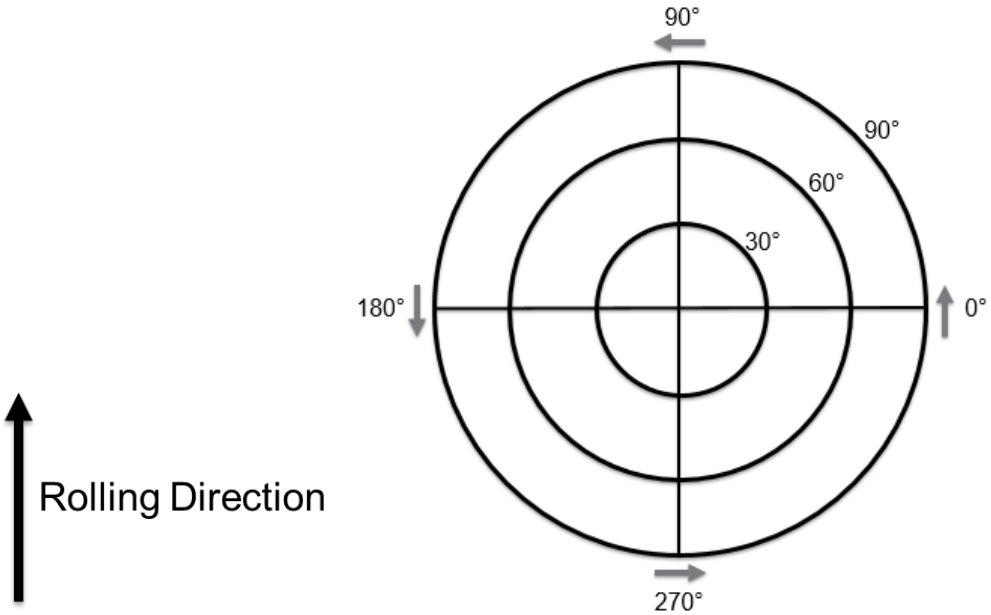

Figure 2.2. The angles the sample was rotated and tilted through to create a pole figure with a constant 2 theta angle. The concentric circles represent the tilt of the sample, with each angle of tilt rotated through a 360° rotation.

3. RESULTS

3.1. HOT BAND CHARACTERIZATION AND CARBIDE CALCULATION

The hot band was coiled at 593°C, which resulted in a bainitic microstructure. Figures 3.1 and 3.2 show low magnification and high magnification images of the as-received CASTRIP hot band microstructure. Tensile properties for the hot band are shown in Table 3.1. The steel did not show a distinct yield point, meaning that the steel exhibits continuous yielding behavior. Figure 3.3 shows the carbide formation calculated in FactSage using the FSstel database for the first 85% liquid composition. Figure 3.4 shows the same calculation for the last 15% liquid. The two carbide types predicted by FactSage are $M_{23}C_6$ and M_6C carbides. For the last 15% liquid, the composition with respect to temperature of the $M_{23}C_6$ carbides is shown in Figure 3.5. The M_6C carbides did not show a dependence on temperature. A typical composition for the M_6C carbides is shown in Table 3.2.

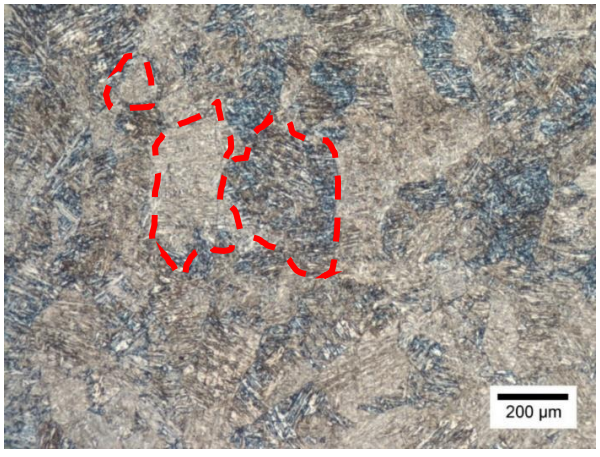

Figure 3.1. Low magnification micrograph of the CASTRIP hot band microstructure. Examples of prior austenite grains are outlined with red dashed lines.

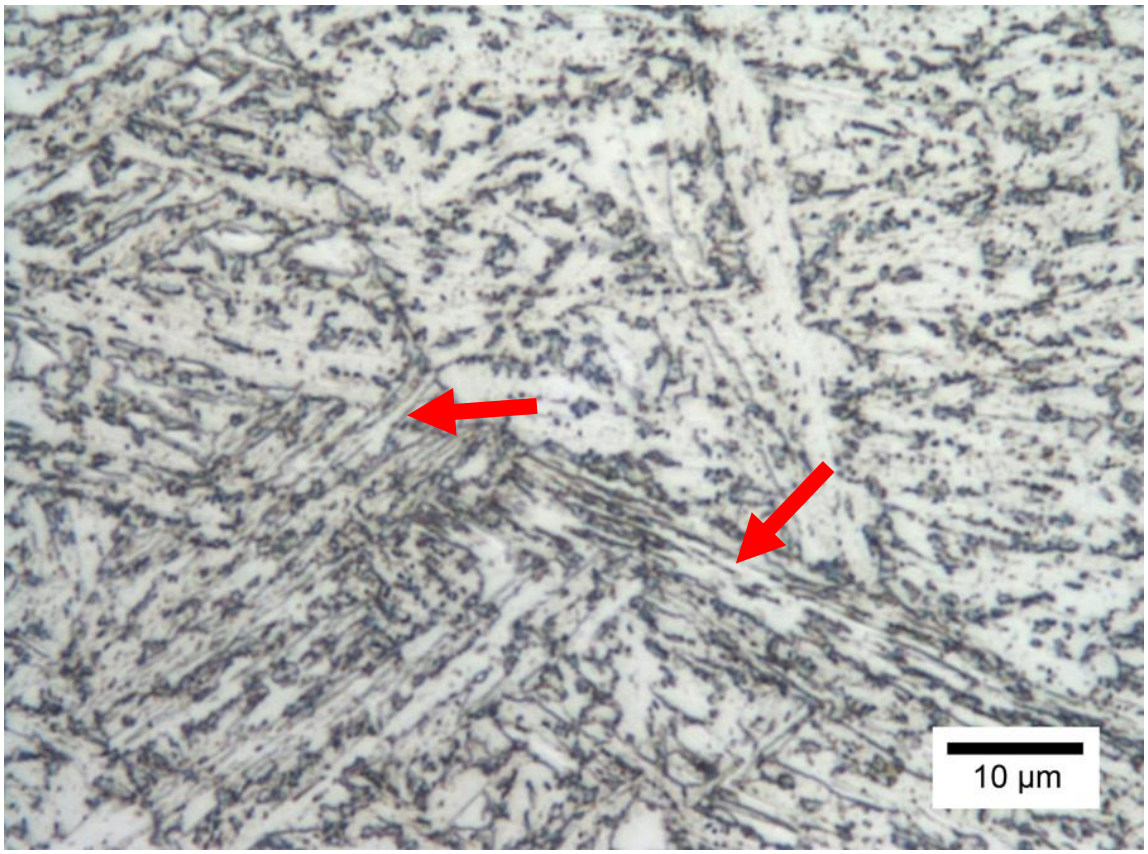

Figure 3.2. As-received CASTRIP hot band microstructure. The microstructure is bainitic. Acicular ferrite structures are indicated by red arrows.

Table 3.1. Tensile properties for the as-received CASTRIP hot band. Each value is an average of three tensile tests.

Material	UTS (MPa)	YS (MPa)	Elongation (%)
CASTRIP Hot Band	1040	663	10.5

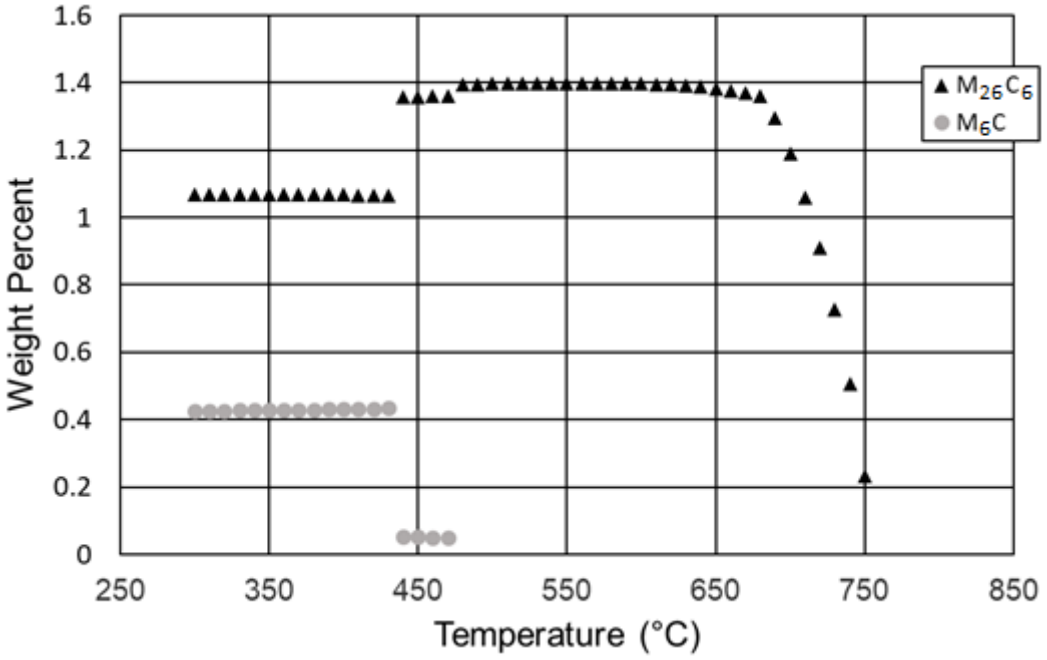

Figure 3.3. Weight percent of $M_{23}C_6$ and M_6C carbides predicted by FactSage for the first 85% liquid to solidify.

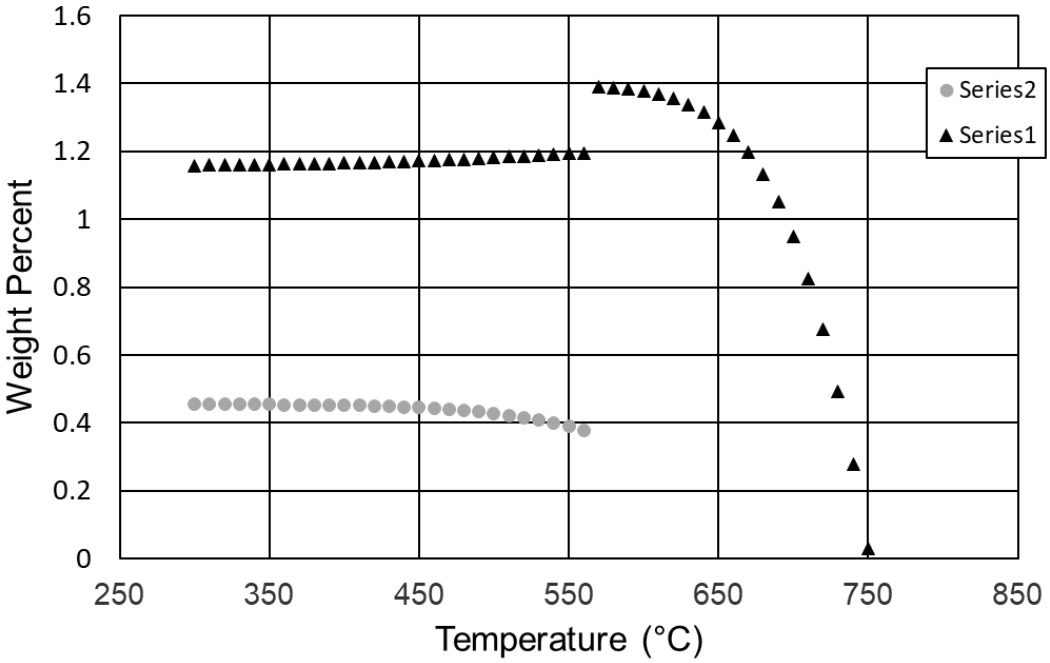

Figure 3.4. Weight percent of $M_{23}C_6$ and M_6C carbides predicted by FactSage for the last 15% liquid to solidify.

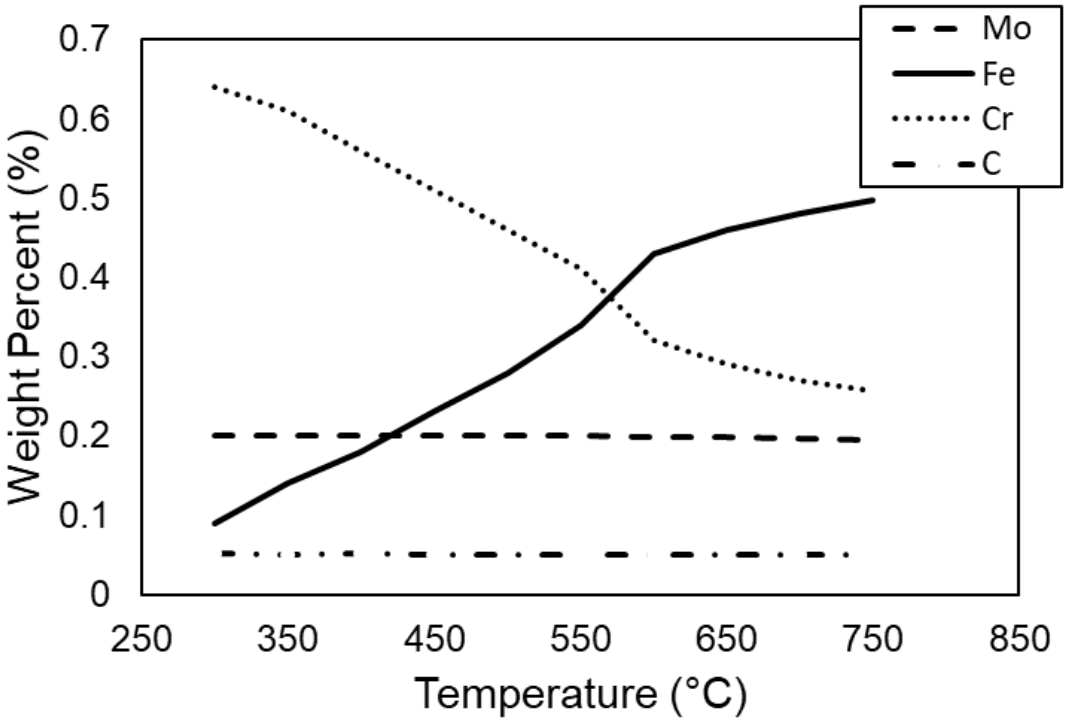

Figure 3.5. Composition of the $M_{23}C_6$ carbides predicted by FactSage for the last 15% liquid to solidify.

Table 3.2. Typical composition of the M_6C carbides.

	Mo	Fe	C
Weight Percent (%)	0.75	0.22	0.024

3.2. INTERCRITICAL REGION

FactSage equilibrium simulations were conducted using the nominal steel composition provided by CASTRIP. At equilibrium, the Ae_1 was calculated to be 675°C and the Ae_3 was calculated to be 825°C. FactSage simulation results (version 7.1, using FSstel database) are shown in Figure 3.6. Table 3.3 shows a comparison between the

FactSage simulation and a 30-minute isothermal heat treatment of the CASTRIP hot band at 700, 725, 770, and 800°C. The percent austenite for each of these experiments was determined with ImageJ measurements of the volume percent martensite seen in micrographs taken of the 4 different heat treatment conditions. Based on the isothermal heat treatments, the intercritical region is approximately 35°C lower than the FactSage prediction for measurements at 700, 725, and 770°C. At 800°C, the experimental percent austenite was within 3% of the predicted amount of austenite.

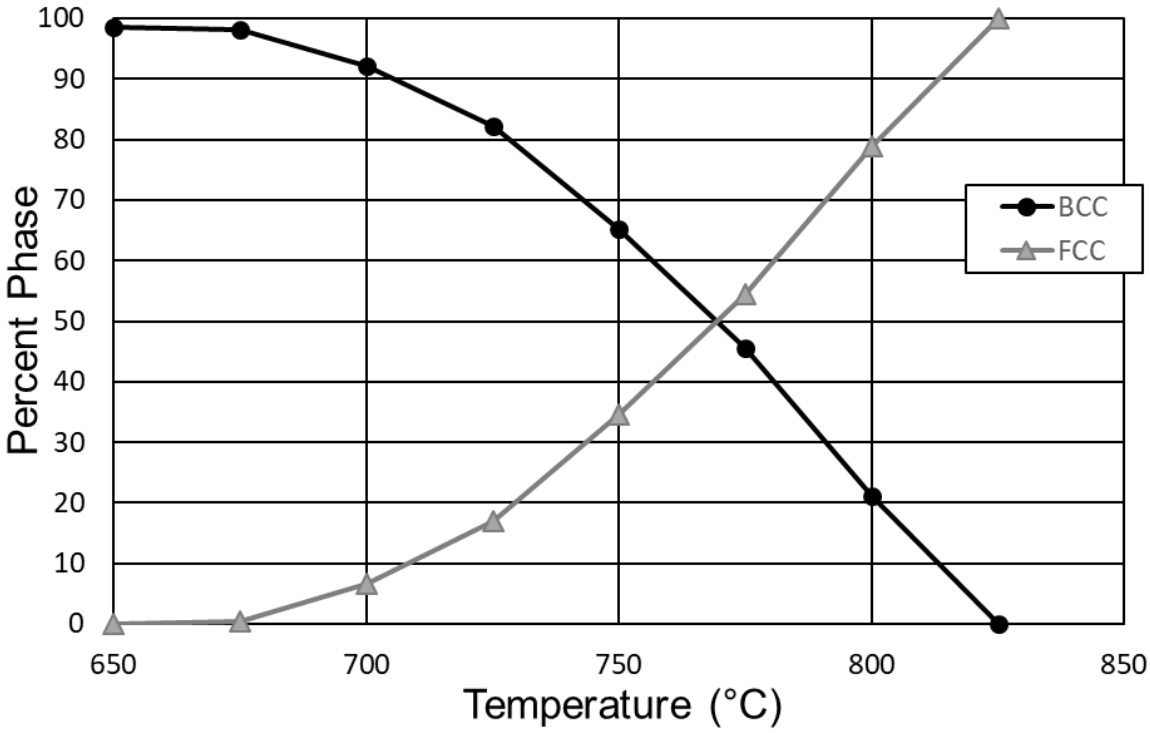

Figure 3.6. Equilibrium FactSage simulation results. The steel composition was provided by CASTRIP. The black line (BCC) represents the ferrite present in the microstructure, and the grey line (FCC) represents the austenite present as the temperature is increased.

Further investigation of the intercritical region was performed using resistivity and temperature measurements as the steel was heated to 900°C at a heating rate of 16 C°/sec. The heating rate in the data provided by CASTRIP for a typical galvanization cycle is 10.3 C°/sec. Four changes in slope for both the temperature data and resistivity data is depicted by the vertical red lines shown Figure 3.7. The first change of slope at 714°C (1317°F) in the temperature and resistivity data is the Ac_1 temperature. The last change of slope at 859°C (1578°F) is the Ac_3 temperature. Table 3.4 shows a comparison between the experimental austenite start and finish temperatures and the FactSage equilibrium austenite start and finish temperatures.

Table 3.3. Experimental and simulated percent austenite in CASTRIP hot band.

Temperature (°C)	% Austenite (Experimental)	% Austenite (Factsage)
800	82	79
770	65	50
725	42	17
700	21	7

Table 3.4. Comparison between equilibrium FactSage results and experimental results for the austenite start and finish temperatures of the CASTRIP hot band.

Critical temperature	Factsage	Experimental (16C°/s)
A1 (°C)	675	714
A3 (°C)	825	859

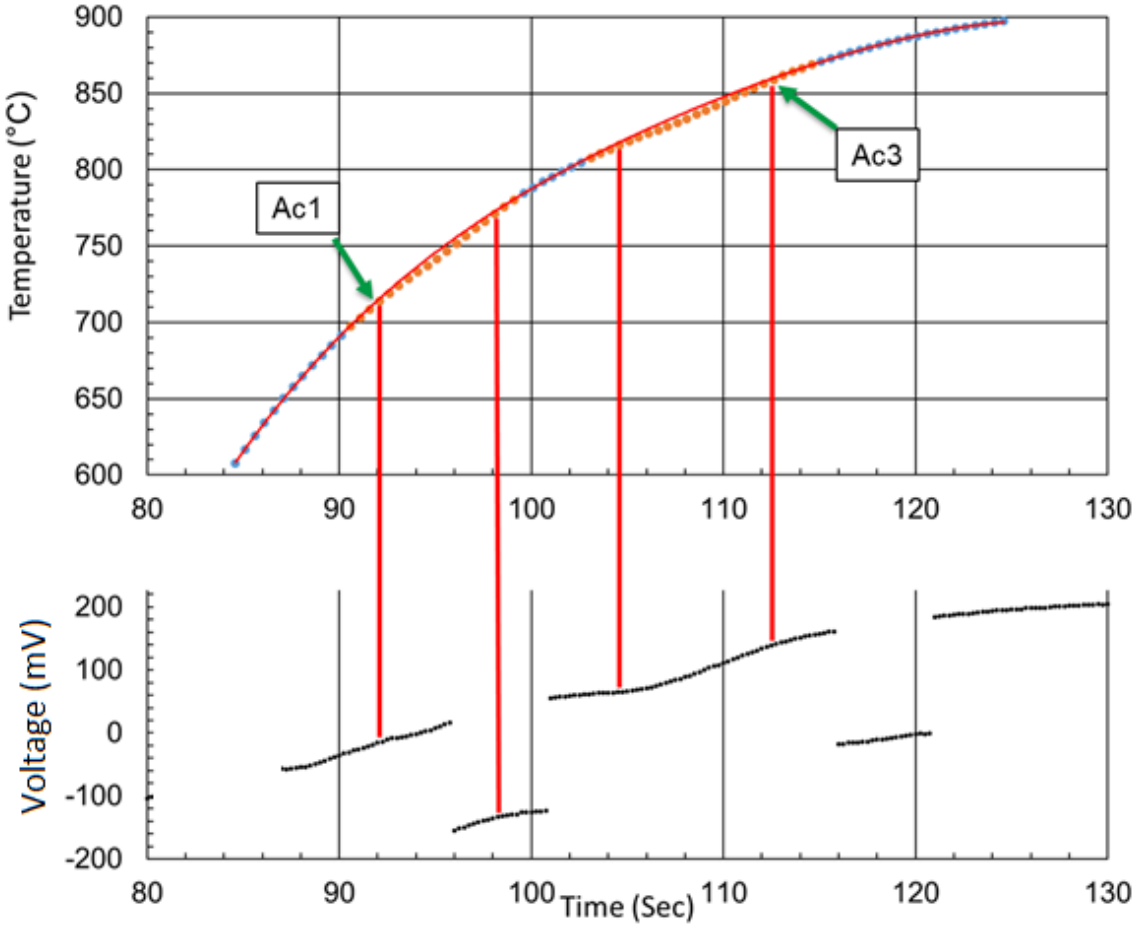

Figure 3.7. Voltage and thermocouple data on samples batch annealed at 649°C for 48 hours, cold rolled to a 20% reduction, and inserted into a furnace with an inert argon atmosphere at 900°C heated at 16°C/sec. The change in slope of the temperature data is indicated by vertical red lines. This corresponds to the change in slope of the voltage data. The start and end points of the changes of slope are associated with the Ac1 and Ac3 temperature of the material. This method yields an experimental Ac1 temperature of 714°C (1317°F) and an Ac3 temperature of 859°C (1578°F)

3.3. ISOTHERMAL HEAT TREATMENTS

Figures 3.8, 3.9, and 3.10 show the microstructures of as-received steel (0% cold reduction), 20% cold reduction, and 65% cold reduction. Each of the three conditions were subjected to a heat treatment of 725°C for 30 min, followed by quenching in water.

The microstructure in Figure 3.5 is comprised of type A austenite forming along lath positions. Figure 3.6 is almost entirely type A austenite, with small amounts of type B austenite growing along prior austenite grain boundaries. The Type A austenite shown in Figure 3.6 is thicker than the Type A austenite shown in Figure 3.5 and does not strictly follow the interlath positioning seen in Figure 3.5. Figure 3.7 is almost entirely type B austenite.

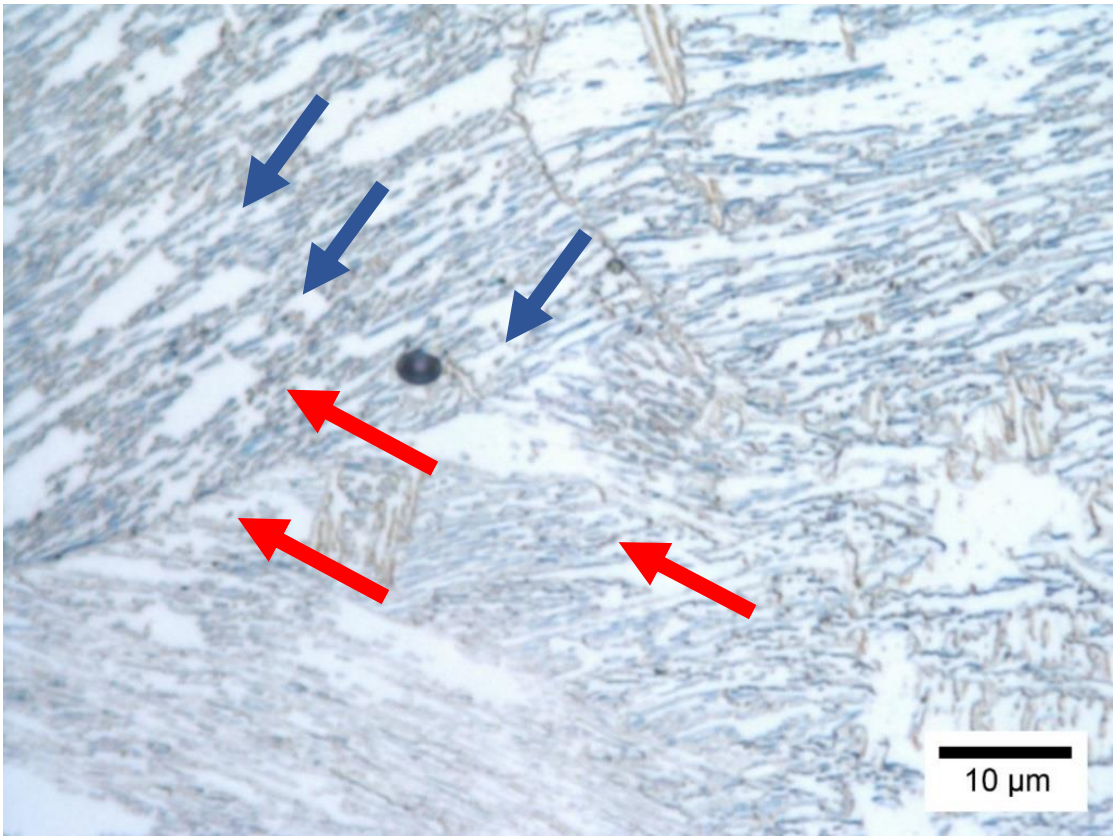

Figure 3.8. Longitudinal view of the microstructure produced by heat treating the as-received steel (0% cold reduction) for 30 minutes at 725°C and quenching in water. The dark phase (red arrows) is type A austenite that has been transformed to martensite after quenching. The ferrite matrix is denoted with blue arrows.

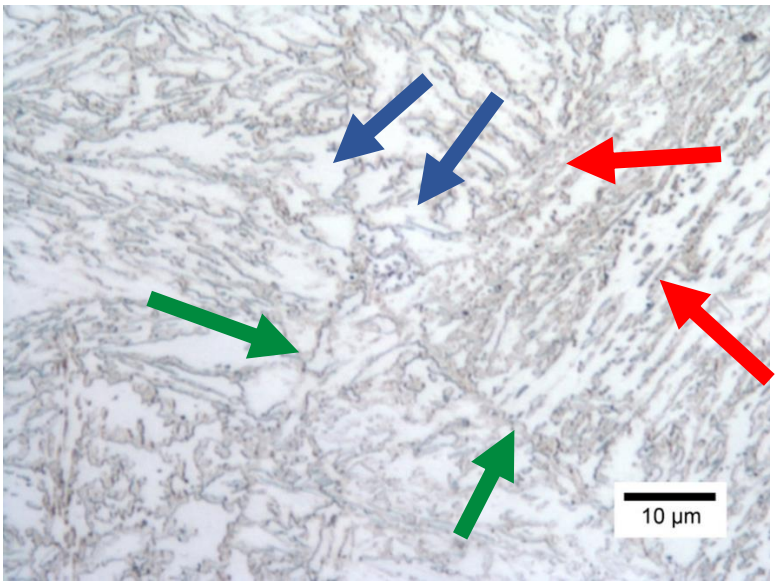

Figure 3.9. Longitudinal view of the microstructure produced by rolling the steel to a 20% cold reduction followed by a 30-minute isothermal heat treatment at 725°C. The steel was quenched in water after heat treating. Red arrows indicate type A austenite that has been transformed to martensite after quenching. Type B austenite is indicated with green arrows. The ferrite matrix is denoted with blue arrows.

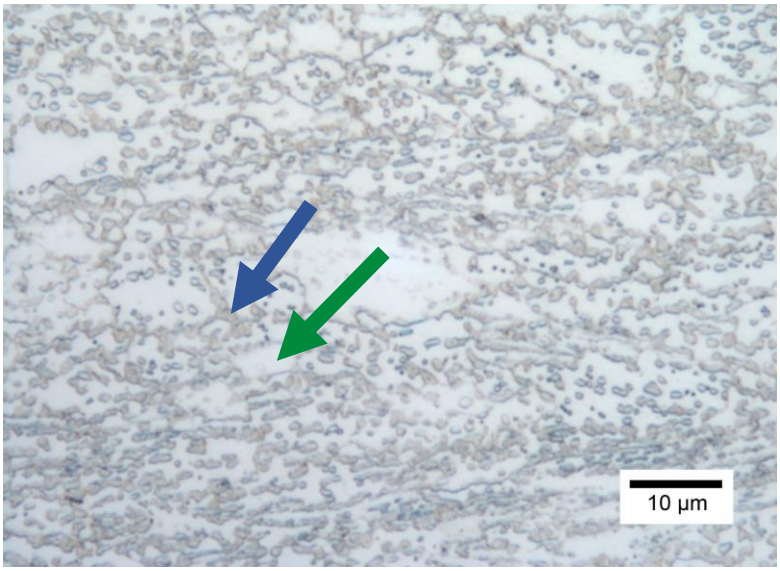

Figure 3.10. Longitudinal view of the dual phase microstructure produced by cold rolling to a 65% reduction, followed by an intercritical heat treatment of 725°C for 30 minutes. The light phase is ferrite (blue arrow) and the dark phase is type B austenite that has transformed to martensite (green arrow).

Table 3.5 shows the mechanical properties of the isothermal heat treatments of the CASTRIP hot band at 700°C, 725°C, 775°C, 800°C and 1000°C. Table 3.6 shows the mechanical properties for steel that was either cold rolled to a 20% reduction or cold rolled to a 65% reduction prior to heat treatment. With the exception of the 700°C treatment, cold rolling to a 20% reduction significantly increases the tensile strength and the yield strength of the steel. Rolling to a 65% reduction showed the best combination of strength and ductility, and was the only heat treatment that met DP 980 tensile requirements. The percent martensite formed in these experiments is similar to the values shown in Table 3.3.

Table 3.5. Mechanical properties of 30 minute isothermal heat treatments of the CASTRIP hot band.

Rolling	Heat Treatment	HRC 0% Red.	UTS (MPa)	YS (MPa)	Elong. (%)
0% Cold Reduction	1000°C (1832°F) Quench	34.3 ± 1.7	-	-	-
	1000°C (1832°F) Air-cool	31 ± 5.9	-	-	-
	800°C (1472°F) Quench	35.3 ± 2.5	1095	793	3.9
	770°C (1418°F) Quench	31 ± 5.9	1028	729	5.1
	725°C (1337°F) Quench	26.6 ±5.8	986	719	6.5
	700°C (1292°F) Quench	25.4 ± 2.5	929	749	6.2

Table 3.6. Mechanical properties of isothermal heat treatments for material that was rolled to a 20% cold reduction and a 65% cold reduction prior to heat treatment.

Rolling	Heat Treatment	HRC	UTS (MPa)	YS (MPa)	Elongation (%)
20% Cold Reduction	800°C (1472°F) Quench	39 ± 0.72	1212	960	2.9
	770°C (1418°F) Quench	36.1 ± 0.66	1160	915	4.7
	725°C (1337°F) Quench	28.8 ± 2	1074	776	4.9
	700°C (1292°F) Quench	27.4 ± 1	911	817	5.9
65% Cold Reduction	750°C (1382°F)	-	1047	596	9.6

3.4. BATCH ANNEALING

Figure 3.11 shows a micrograph of as-received CASTRIP steel that was subcritically annealed at 649°C (1200°F) for 48 hours. A 48 hour thermal cycle simulated a typical batch anneal cycle of a hot band coil. The dark areas in the image show the carbide coarsening throughout the microstructure, both on grain boundaries and at interlath positions. The batch annealing cycle also resulted in some ferrite recrystallization. As a result of the subcritical annealing, the cold rolling force was reduced by approximately 21.5% in comparison to CASTRIP hot band. A 9% cold gauge thickness reduction required 138 MPa of force for the as-received steel, while a 12% cold reduction of the batch annealed steel required 108 MPa of force. The difference in reduction is a result of the rolling mill compliance under different loads.

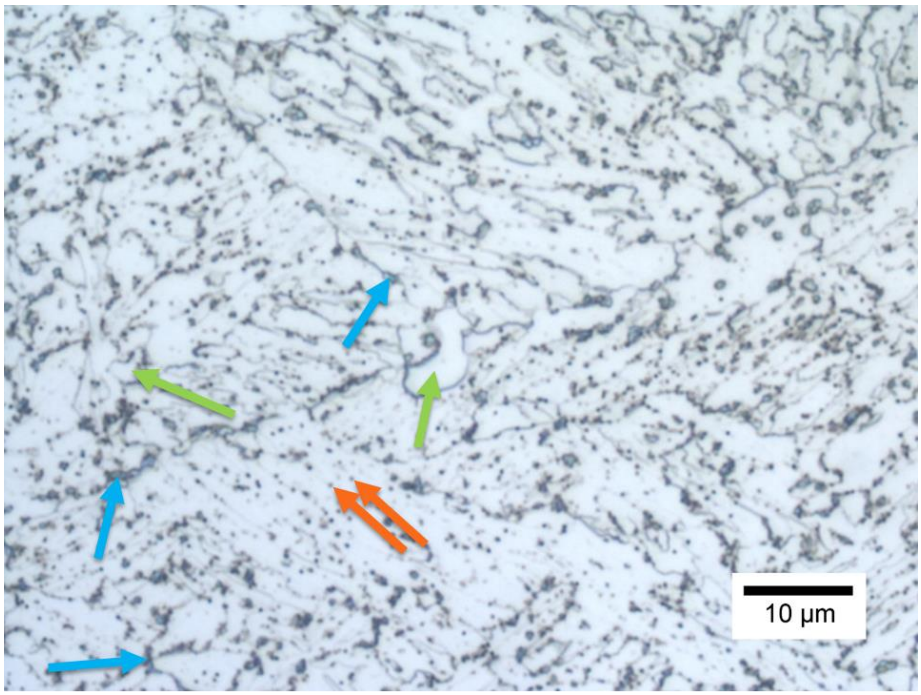

Figure 3.11. Microstructure resulting from batch annealing at 649°C for 48 hours. Instead of the bainitic structure in the CASTRIP hot band (Figure 3.1 and 3.2), the microstructure is comprised of a carbide-containing ferrite matrix. Carbide nucleation and growth has taken place on grain boundaries (blue arrows) and on interlath positions (orange arrows). Some ferrite recrystallization has taken place (green arrows).

3.5. DYNAMIC STRAIN AGING

Warm rolling was investigated to determine if dynamic strain aging would induce recrystallization at the maximum 20% reduction imposed by the CASTRIP product. Figure 3.12 shows the results of a typical tensile test of the CASTRIP hot band at 100°C at a strain rate of 0.01 s^{-1}. At 100°C no dynamic strain aging was observed, as indicated by the lack of serrations in the stress-displacement curve. Figure 3.13 shows a strong dynamic strain aging effect for a single tensile test conducted at 300°C at a strain rate of 0.01 s^{-1}. Figure 3.14 shows an Arrhenius plot created by compiling the dynamic strain

aging tests. If dynamic strain aging was observed, it was designated by a green dot on the plot. If dynamic strain aging was not observed, it was designed by a red dot. The boundary between the two regions is shown by the black line in the plot. Based upon the slope of the line in this graph, an activation energy for the onset of dynamic strain aging was found to be 84 kJ/mol. From this data, it was determined that warm rolling at 500°C would induce dynamic strain aging in the steel, as that falls well within the region of the plot where dynamic strain aging is observed.

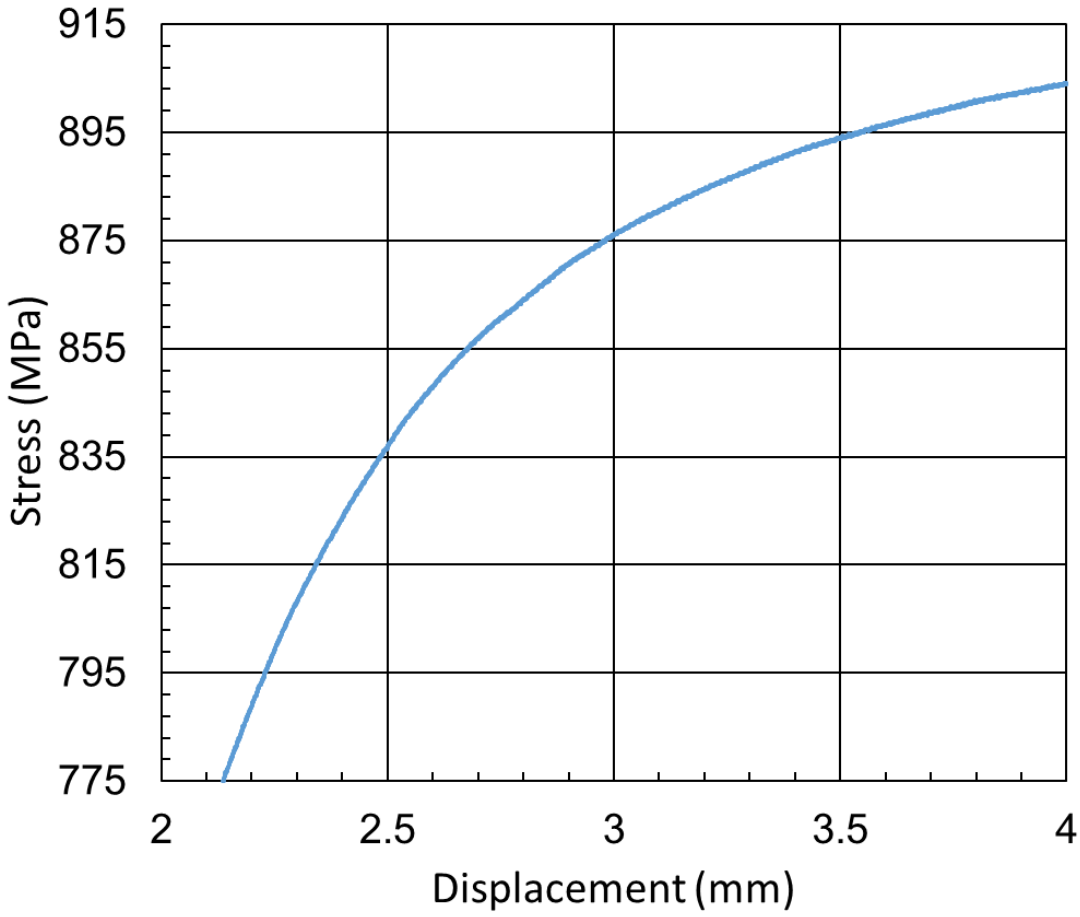

Figure 3.12. Tensile results for a test at 100°C at a strain rate of 0.01 s^{-1}. The lack of serrations indicate that no dynamic strain aging has occurred in this sample.

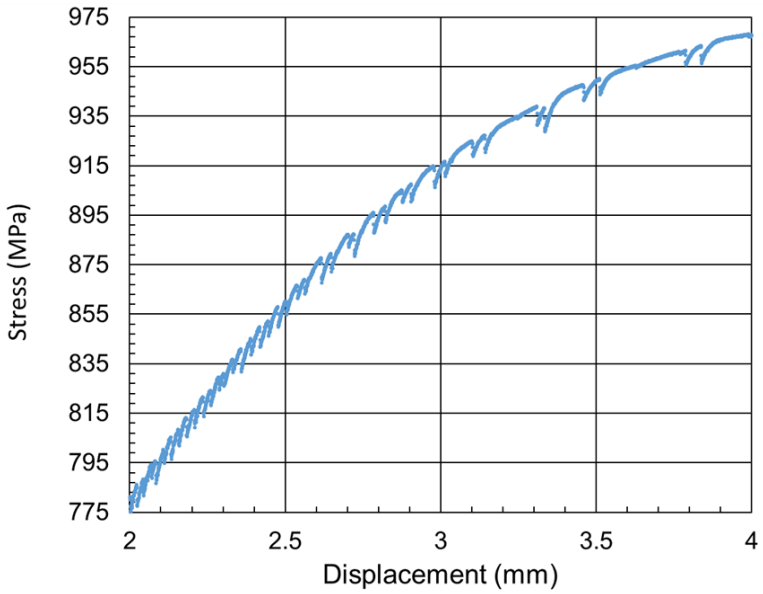

Figure 3.13. Serrations in the stress-displacement curve 300°C at a strain rate of 0.01 s^{-1}. These serrations demonstrate the dynamic strain aging effect at this specific strain rate and temperature.

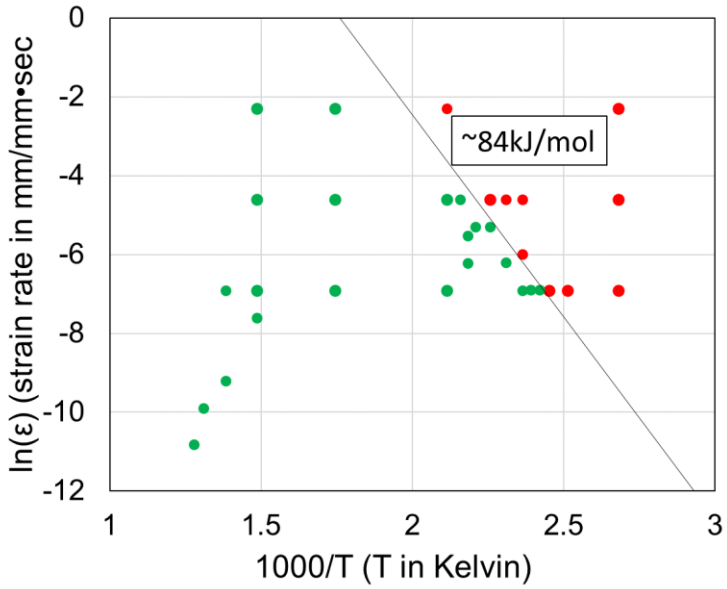

Figure 3.14. Arrhenius plot of the dynamic strain aging effect in CASTRIP steel. The red dots indicate a tensile test that did not exhibit dynamic strain aging. The green dots indicate that dynamic strain aging occurred in that specimen.

3.6. MECHANICAL PROPERTIES AND MICROSTRUCTURE

Table 3.7 shows the tensile results for steel that was batch annealed, cold or warm rolled at 500°C to a 20% reduction, and continuously annealed per Figure 2.1. For comparison, the mechanical properties of steel that was cold rolled to a 20% reduction and isothermally heat treated at 725°C is shown at the top of the table. Each of the tensile results reported in Table 3.7 is an average of three tensile tests. The material that was warm rolled in dynamic strain aging conditions prior to the continuous annealing at 810°C did not exhibit significantly different mechanical properties from the cold rolled steel. Steel that was batch annealed, cold or warm rolled to a 20% reduction, and continuously annealed produced mechanical properties that met ASTM A1079 criteria for DP 980 steel.

Figure 3.15 shows the microstructure for the CASTRIP hot band that was continuously annealed at 760°C. The continuously annealed CASTRIP hot band microstructure shows Type A austenite formation, with a very small amount of Type B austenite formation. Figure 3.16 shows the microstructure for steel that was batch annealed at 649°C for 48 hours, cold rolled to a 20% reduction, and continuously annealed at 810°C. Instead of Type A austenite formation, the microstructure in Figure 3.16 shows Type B austenite as the primary form of austenite. Figure 3.17 shows the microstructure produced that was batch annealed at 649°C for 48 hours, warm rolled at 500°C to a 20% reduction, and continuously annealed at 810°C. The microstructure in Figure 3.17 is very similar to the microstructure displayed in Figure 3.16. Both thermomechanical processes produce primarily type B austenite. Qualitatively there appears to be less type A austenite in the warm rolled steel than there is in the cold rolled

steel. However, this does not appear to have a significant impact on the mechanical properties.

Table 3.7. Tensile results from final iterations of annealing, rolling, and continuous annealing. Best isothermal heat treatment results are added for comparison

Sample and Heat Treatment	UTS (MPa)	YS (MPa)	Total Elong. (%)	Unif. Elong. (%)
0% Cold Roll, 725°C (1337°F) for 30 min, Quench	986	719	6.5	-
20% Cold Roll, 725°C (1337°F) for 30 min, Quench	1074	776	4.9	-
65% Cold Roll, 750°C (1382°F) for 30 min, Quench	1047	596	9.6	-
48 hrs at 649°C (1200°F) No Reduction, Cont. Anneal at 810°C (1490°F)	842	631	10	-
48 hrs at 649°C (1200°F) 20% Cold Roll, Cont. Anneal at 810°C (1490°F)	1038	744	8.6	6
48 hrs at 649°C (1200°F), 20% Warm Roll, Cont. Anneal at 810°C (1490°F)	1030	736	8.9	6
CASTRIP Hot Band Cont. Anneal at 760°C (1400°F)	1123	790	9.6	-
CASTRIP Hot Band Cont. Anneal at 810°C (1490°F)	968	672	3.8	-
ASTM A1079: DP 980	Min 980	Min 550	Min 8	-

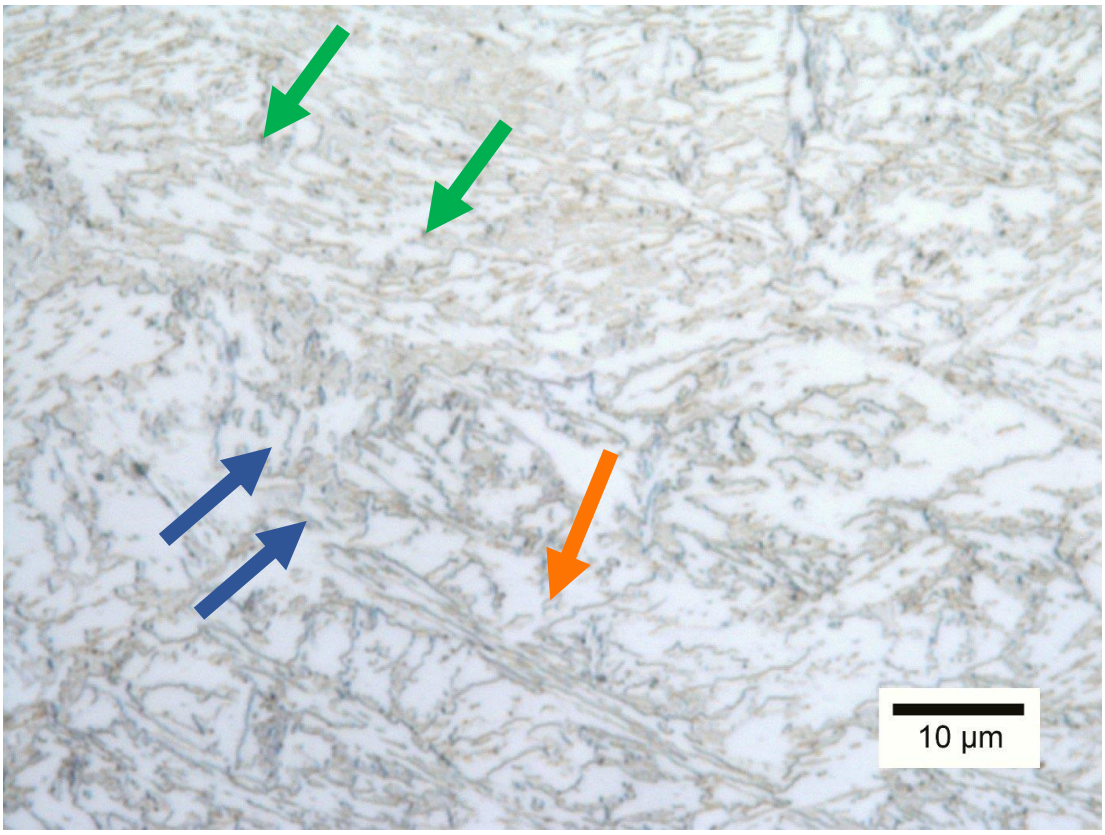

Figure 3.15. Microstructure resulting from continuous annealing CASTRIP hot band with an intercritical temperature of 760°C (S-L). A very small amount of Type B austenite (orange arrows) has nucleated on prior austenite grain boundaries. Type A (blue arrows) austenite has nucleated and grown on carbides and interlath positions. Dark spots (green arrows) indicate that either the carbides are not entirely dissolved in the continuous annealing process.

Image J analysis for the steel that was batch annealed, 20% cold rolled, and continuously annealed showed the mean ferrite grain size to be approximately 3.5 µm. The average martensite island diameter was found to be approximately 1.7 µm. The volume percent of martensite is approximately 60%. Steel that was batch annealed, 20% warm rolled, and continuously annealed had a mean ferrite grain size of approximately 3.8 µm. For this steel, the average martensite island diameter was approximately 1.7 µm and the volume percent of martensite is 61%.

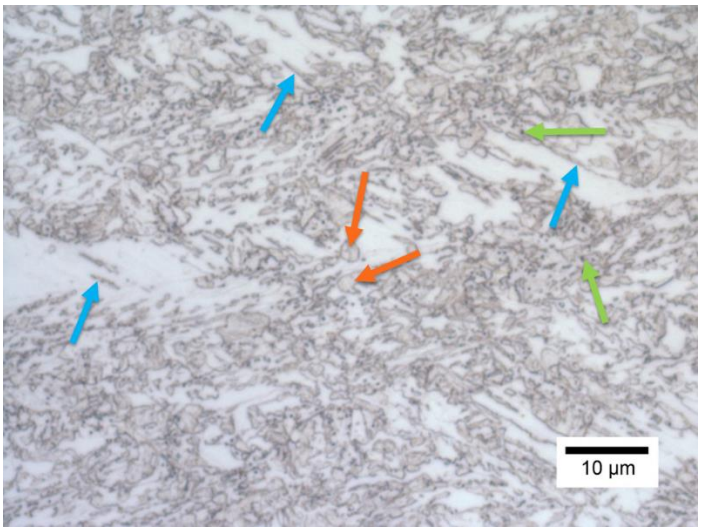

Figure 3.16. Microstructure resulting from batch annealing at 649°C (1200°F) for 48hrs, cold rolling to a 20% reduction, and continuous annealing at 810°C (S-L). Type B (orange arrows) and Type A (blue arrows) austenite has nucleated and grown on carbides and interlath positions, as well as grain boundaries. Dark spots (green arrows) indicate that either the carbides are not entirely dissolved in the continuous annealing process.

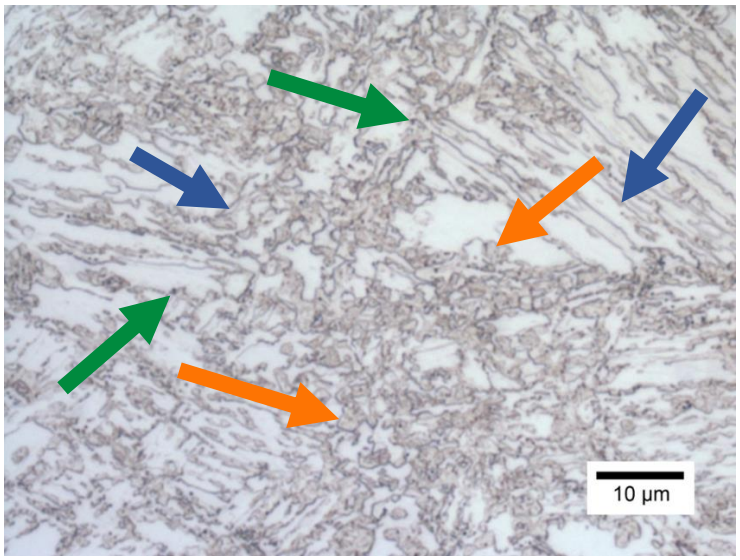

Figure 3.17. Microstructure resulting from batch annealing at 649°C (1200°F) for 48hrs, warm rolling to a 20% reduction, and continuous annealing at 810°C (S-L). Type B (orange arrows) and Type A (blue arrows) austenite has nucleated and grown on carbides and interlath positions, as well as grain boundaries. Dark spots (green arrows) indicate that either the carbides are not entirely dissolved in the continuous annealing process.

3.7. TEXTURE ANALYSIS

Figure 3.18 compares the {110} pole figure between (a) CASTRIP hot band, (b) steel that was batch annealed, warm rolled at 500°C to a 20% reduction and continuously annealed at 810°C, and (c) steel that was cold rolled to a 65% reduction and isothermally heat treated at 750°C for 30 minutes. Although there is clearly some texturing in (a) and (b), the majority of the grains are randomly oriented. The texture seen in the {110} pole figures is a partial γ fiber, with the maxima close to the idea texture of {111}<112>, a common texture in rolled and recrystallized steels. Another component that is represented is the cubic {100}<110> texture as seen in the 200 pole figures (Figure 3.19). No significant difference was observed between the CASTRIP hot band and the steel that was batch annealed, warm rolled at 500°C to a 20% reduction and continuously annealed at 810°C. However, the steel that was cold rolled to a 65% reduction and isothermally heat treated at 750°C for 30 minutes shows a much stronger γ fiber running from {111}<110> to {111}<112>.

Figure 3.20 shows the Vickers hardness results across the width of a sheet that was cold rolled to a 20% reduction and a sheet warm rolled at 500°C to a 20% reduction. There is an approximate average increase of 10 Vickers from the cold rolled sheet to the warm rolled steel. This converts to an increase of 1.2 HRC.

Figure 3.21 shows the differential scanning calorimetry results for steel that was batch annealed at 649°C for 48 hours and cold rolled to a 20% reduction. Figure 3.22 shows the differential scanning calorimetry results for steel that was batch annealed at 649°C for 48 hours and warm rolled at 500°C to a 20% reduction. The area between the curves of the cold rolled sample is approximately 2.7 mW/mg. The area between the

curves of the warm rolled sample is approximately 11 mW/mg. Figure 3.23 shows the difference curves of the two different conditions. This visually represents the difference in heat evolved between the two different processing conditions.

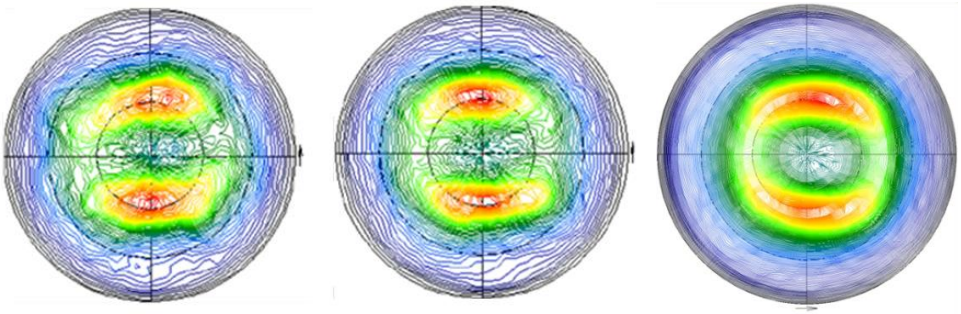

(a) (b) (c)

Figure 3.18. A comparison of {110} pole figures for the CASTRIP hot band (a), batch annealed, warm rolled, and continuously annealed at 810°C (b). The steel was also cold rolled to a 65% reduction and isothermally heat treated at 750°C for 30 minutes (c). For (a) and (b), peaks in intensity are at an angle of approximately 30° and are indicated by red contour lines. This indicates there is a partial γ fiber present, with a maxima at a {111}<112> orientation.

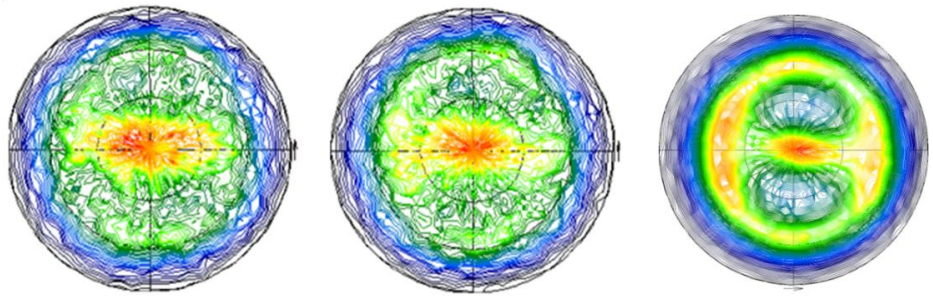

(a) (b) (c)

Figure 3.19. A comparison of {200} pole figures for the CASTRIP hot band (a)), batch annealed, warm rolled, and continuously annealed at 810°C (b). The steel was also cold rolled to a 65% reduction and isothermally heat treated at 750°C for 30 minutes (c). In (a) and (b), there is a mild cubic texture present. The lack of a {111}<112> peak in (a) and (b) indicates that the γ fiber is also very mild.

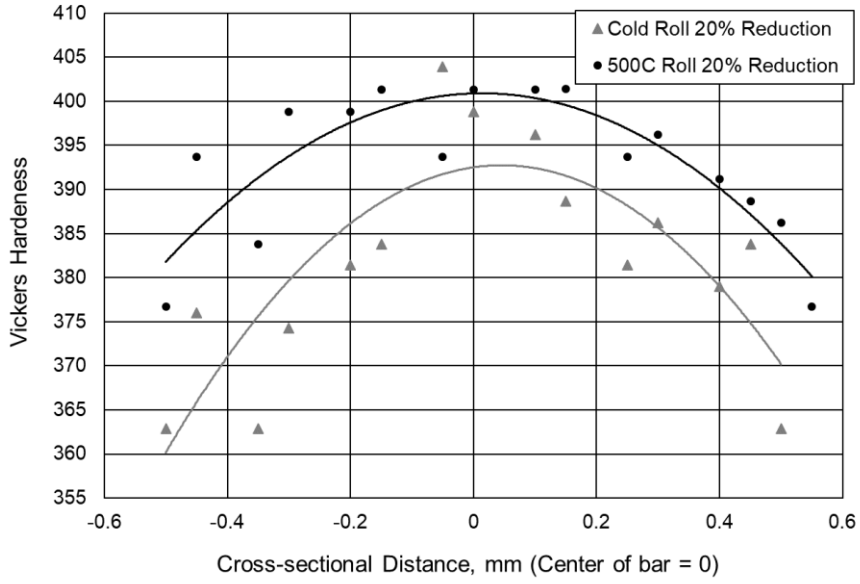

Figure 3.20. Vickers hardness results across the width of a sheet of cold rolled steel and a sheet of warm rolled steel. The center of the sheet is designated as 0.

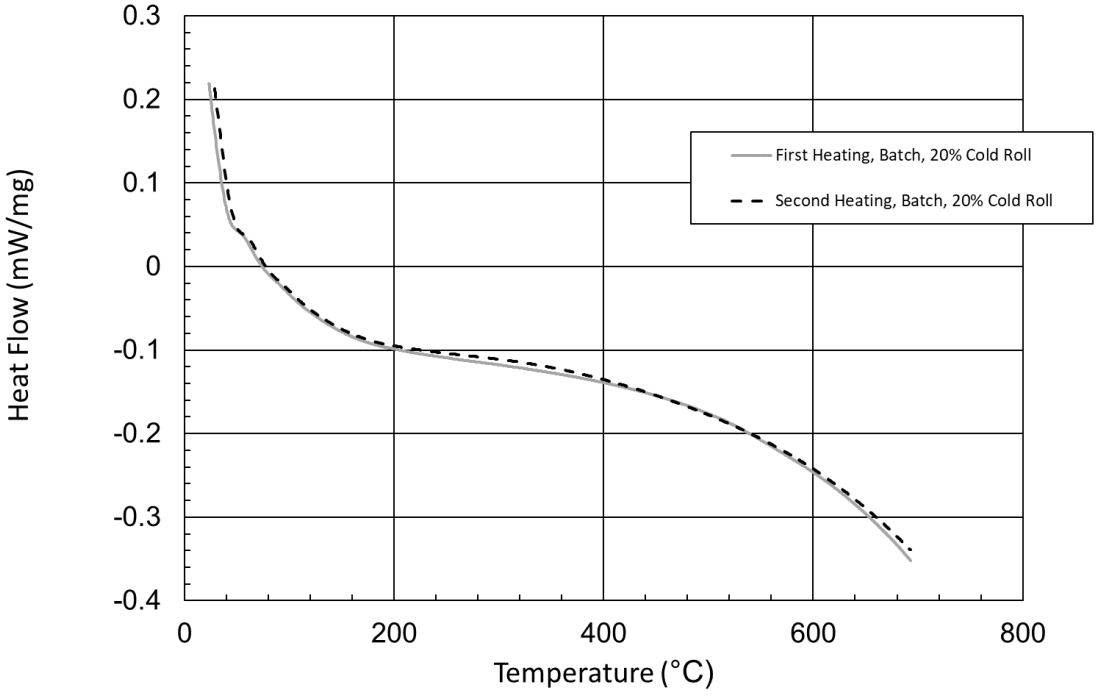

Figure 3.21. Differential scanning calorimetry results for heat flow of the batch annealed and cold rolled steel.

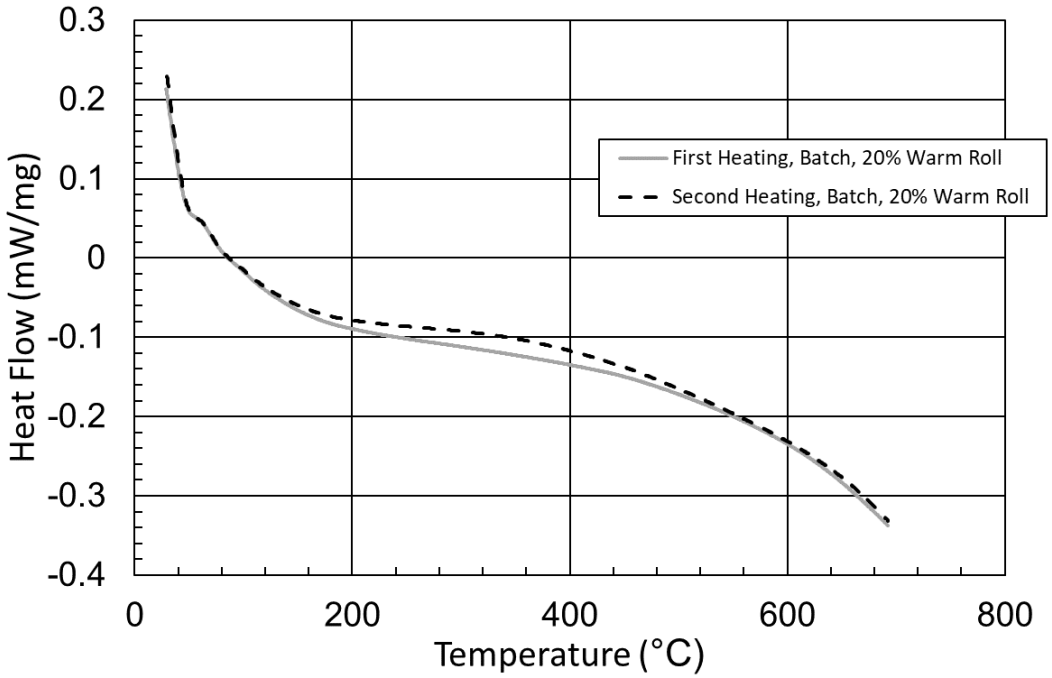

Figure 3.22. Differential scanning calorimetry results for heat flow of the batch annealed and warm rolled steel.

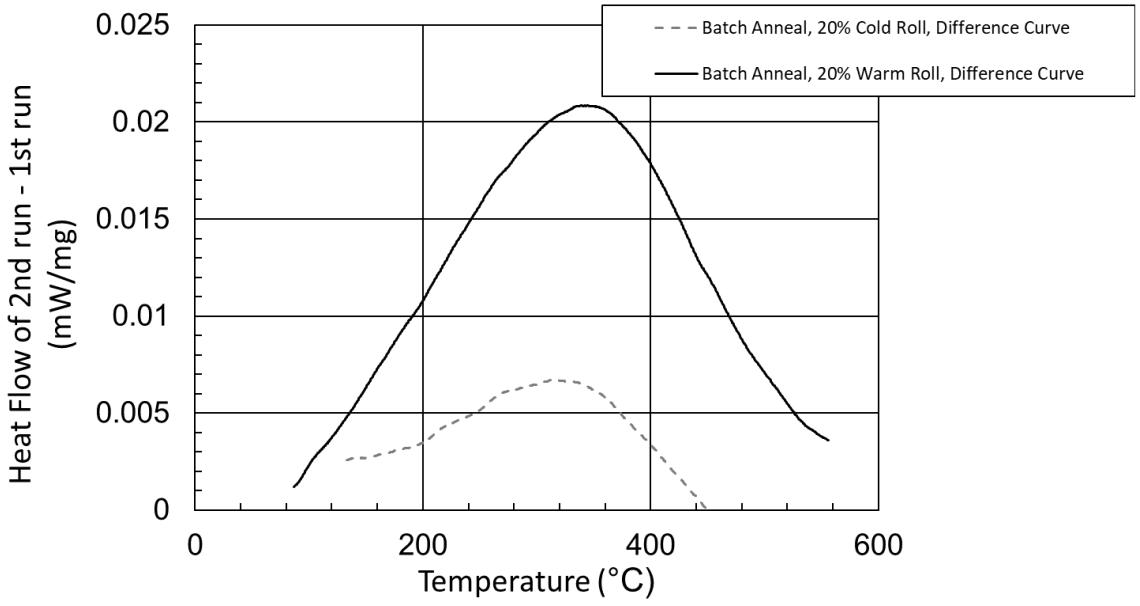

Figure 3.23. Difference curves comparing the differential scanning calorimetry results for heat flow of the batch annealed and either cold or warm rolled steel.

4. DISCUSSION

4.1. FINAL THERMOMECHANICAL PROCESSING CYCLE

CASTRIP hot band tensile properties meet ASTM A1079 DP 980. Since the microstructure is bainitic, it is not considered dual phase steel. Continuously annealing CASTRIP hot band at an intercritical temperature of 760°C also met DP 980 requirements, as recorded in Table 3.7. Figure 3.16 and Figure 3.17 show that batch annealing and warm or cold rolling to a 20% reduction prior to continuously annealing qualitatively improved the percentage of Type B austenite present in the steel. However, the continuously annealed CASTRIP hot band showed a superior tensile strength and elongation in comparison to the steel that was batch annealed and cold or warm rolled to a 20% reduction prior to continuous annealing at 810°C (Table 3.7). Although continuous annealing at 760°C of the CASTRIP hot band formed almost entirely Type A austenite, the austenite formation remained discrete. This discrete austenite formation caused the increase in ductility seen between the CASTRIP hot band that was isothermally heat treated at 725°C and the CASTRIP hot band that was continuously annealed at 760°C.

A lower intercritical temperature of 760°C was required for continuously annealing the CASTRIP hot band in comparison to continuous annealing the thermomechanically processed steel at 810°C. Continuous annealing the CASTRIP at 810°C showed an elongation of 3.8%, in contrast to the 9.6% elongation produced by continuously annealing the hot band at 760°C as recorded in Table 3.7. The decrease in elongation indicates that it is possible that the martensite structure had become interconnected at an intercritical temperature of 810°C. This is likely due to a change in

austenite formation kinetics, since the starting microstructure of the CASTRIP hot band is bainitic, while the starting microstructure of the thermomechanically processed material was a carbide-containing ferrite matrix. Research by Speich et al. shows that the dissolution of pearlite is very rapid during austenite growth, and grain growth slows once the austenite begins growing into the ferrite matrix as a result of the carbon diffusion path increasing in distance [88]. If the carbides become alloyed during the subcritical heat treatment, these carbides will dissolve much slower than the carbides formed in the CASTRIP hot band, causing the austenite to grow more quickly in the CASTRIP hot band.

Cold rolling the batch annealed steel to a 20% reduction prior to continuous annealing at 810°C will increase the tensile strength by 196 MPa and the yield strength by 113 MPa in comparison to heat treating the batch annealed steel without any reduction. The four isothermal heat treatments also show an increase in the tensile strengths and the yield strengths, as reported in Tables 3.5, 3.6, and 3.7. The difference in strength between the two conditions is caused by the more globular austenite formation as a result of additional nucleation sites created by cold rolling to a 20% reduction. The difference in microstructure can be seen in Figure 3.5 and Figure 3.6. The decrease in ductility in the steel cold rolled to a 20% reduction prior to isothermally heat treating at 725°C for 30 minutes is likely due to the interconnected austenite formations along prior austenite grain boundaries as recorded in Figure 3.6. This agrees with the work of He et al. and Kim and Thomas, who found that an interconnected martensite structure showed a significantly lower elongation than microstructures with discrete martensite [77, 78].

Cold rolling CASTRIP hot band to a 65% reduction and isothermally heated treating showed that a dual phase microstructure with discrete Type B martensite islands can be achieved. As a result of the Type B austenite formed, these samples had the best combination of strength and ductility. The yield strength for this steel was 596 MPa, which is approximately 145 MPa less than the yield strength produced by the other thermomechanical processes that met DP 980 mechanical property standards. Reducing the yield strength of the steel is desirable if the steel will be subject to additional forming, since it will reduce the force needed to form a given part. Pole figures of the steel that was cold rolled to a 65% reduction and isothermally heat treated at 750°C for 30 minutes contain a significant γ-fiber. This is expected, based upon the discussion of texture in section 1.2.7.

CASTRIP hot band is 1.5 mm thick (0% reduction). At a 65% reduction, the steel is 0.6 mm thick. Tensile results for 65% reductions may not be comparable to samples of the 20% or 0% reductions. Reducing the thickness of the sample can reduce the strength and ductility of the material if the ratio of sample size to grain size becomes significant. According to the work of Suh et al., in aluminum tensile specimens the mechanical properties begin to decrease in aluminum samples at a thickness to grain size ratio of 40 [120]. The ratio of grain size to sample thickness for the 65% cold rolled and heat-treated steel is approximately 180. Since this ratio is significantly higher than the ratios reported by Suh et al., it is not possible to confidently say whether the sample thickness to grain size ratio affected the tensile results. At sample thicknesses below 1 mm, Suh et al. also found that the surface roughness of the sample had a significant effect on the tensile properties [120]. Typically elongation is the most adversely affected material property in

thin samples, since surface irregularities will cause early neck formation and a reduced ultimate tensile strength. Thus, it is possible that a thicker sample size of the 65% cold rolled and isothermally heat-treated steel may exhibit greater elongations to failure and higher ultimate tensile strengths than those reported in Table 3.7.

Research by Fonstein shows that a dual phase microstructure with 60% martensite has a tensile strength of 1000 MPa and a yield strength of 770 MPa [47]. This is comparable to the tensile strength of 1038 MPa and yield strength of 744 MPa found for the CASTRIP steel that was batch annealed, cold rolled to a 20% reduction, and continuously annealed at 810°C. For a 60% martensite steel, Fonstein predicts that there will be a uniform elongation of 4%, while the processed CASTRIP steel had a uniform elongation of 6%. This increase in uniform elongation is likely due to the small grain size of the CASTRIP steel. The work of Lanzillotto and Pickering suggests that decreasing the grain size of dual phase steel increases the formability of the steel [79], which would also increase the uniform elongation of the steel.

As discussed in section 1.2.9, Gorni developed equations to predict the mechanical properties of steel based upon the grain size and martensite volume fraction of the steel. However, there is a grain size domain for Gorni's equations. For example, a ferrite grain size of 4 μm is predicted by Gorni to have a uniform elongation of 0%. Since the grain size of the processed CASTRIP steel is less than 4 μm, Gorni's equation are not applicable.

4.1.1. Intercritical Region. Isothermal heat treatments showed the intercritical region to be approximately 35°C lower than FactSage equilibrium simulations of 700, 725, and 700°C. At 800°C it is possible that austenite growth into the ferrite is still

controlled by manganese diffusion. After the initial carbide dissolution takes place, austenite formation controlled by manganese diffusion takes between 4 and 24 hours to reach completion [88]. Thus, it is likely that given more time, the 800°C isothermal heat treatment would also show an increased amount of austenite.

In comparison to the isothermal heat treatments, the resistivity experiments indicated the intercritical region increased in temperature by approximately 70°C. This heating rate is comparable to the heating rate provided by Nucor for a continuous annealing thermal cycle. The increase in intercritical region demonstrates that the intercritical temperature in the steel is sensitive to the heating rate. Thus, when designing continuous annealing cycles for CASTRIP hot band, the heating rate must be considered when choosing an appropriate intercritical temperature.

4.1.2. Development of Batch Annealing. Nucleation sites for type B austenite are typically created by cold rolling the steel to reductions between 50% and 75% [62, 63]. Metallography and tensile results of the CASTRIP steel rolled to a 65% reduction, isothermally heat treated for 30 minutes and quenched, show that it is possible to produce type B austenite in a ferrite matrix that meets ASTM A1079 DP 980 standards (Figure 3.10). However, due to the starting thickness of CASTRIP steel (~1.5mm), the CASTRIP process is limited to a 20% cold reduction. A 20% cold reduction of the CASTRIP hot band is not sufficient to provide nucleation sites for type B austenite formation in these samples**.**

Another method of providing nucleation sites was explored, since cold rolling CASTRIP steel to reductions greater than 20% was not an option Austenite is known to preferentially nucleate on carbides [116]. To grow carbides in the microstructure, batch

annealing at 649°C for 48 hours was added to the beginning of the thermomechanical processing cycle. Metallography shows this created a significant number of carbides within the microstructure that could serve as nucleation sites for discrete type B austenite (Figure 3.11). The intercritical temperature for continuously annealing the batch annealed steel was increased by 40°C to compensate for the change in carbide from cementite to alloy carbide due to batch annealing. Batch annealing reduced the yield strength of the steel by approximately 150 MPa, which decreased the rolling force by 21.5%.

4.1.3. Texture and Dynamic Strain Aging. Previous research indicates that CASTRIP steel has a randomly orientated texture [116]. Thus, to improve the drawability of CASTRIP steel, improvements to the texture must be made. Steel textures are normally improved by cold rolling to significant reductions. For example, mild steels are commonly cold rolled up to a 90% cold reduction, and dual phase steels are commonly cold rolled between 50 and 75%. This aligns the maximum percentage of grains to an orientation that is favorable for drawability. Pole figures of the steel that was cold rolled to a 65% reduction and isothermally heat treated at 750°C for 30 minutes contain a significant γ-fiber (Figures 3.18 and 3.19). However, since CASTRIP is limited to 20% cold reduction, other methods must be utilized. In this study, rolling in dynamic strain aging was investigated as a possible method for increasing the γ-fiber intensity.

The onset activation energy of dynamic strain aging in CASTRIP steel was found to be 84 kJ/mol. Research shows that the activation energy for carbon diffusion in ferrite is 82 kJ/mol [119]. Thus, dynamic strain aging in the CASTRIP steel used in this study is likely controlled by carbon diffusion. Dynamic strain aging is typically avoided in normal rolling practices, since it can produce heavy shear banding. Dynamic strain aging at high

reductions typically accommodates deformation in the steel without rotating the grains to favorable orientations [30, 31]. At the low reductions, it is possible that the extra work created by dynamic strain aging will continue to rotate the grains of the steel instead of producing shear bands.

Warm rolling the steel at 500°C (dynamic strain aging conditions) to a 20% reduction was compared to cold rolling to a 20% reduction. Tensile properties for this experiment do not show a significant difference between the warm rolled and cold rolled steel that was continuously annealed. XRD pole figure results show an essentially randomly oriented structure for both experiments (Figures 3.18 and 3.19). However, both Vickers hardness measurements and differential scanning calorimetry results show an increase in hardness and heat flow for the warm rolled steel. This indicates that more work has been put into the steel by rolling in dynamic strain aging conditions. Since the XRD pole figure results indicate that the texture pattern did not change, it is likely that this additional work has been accommodated by the creation of shear bands. However, a careful study of warm rolling at low to medium reductions is needed to verify the precise deformation mechanism present in the steel.

4.1.4. Future Work. Future work for this project should seek to fully understand the difference between cold rolling and rolling in dynamic strain aging conditions at low reductions. This goal could be achieved by combining multiple partial pole figures to form an Orientation Distribution Function (ODF) plot, which would decisively determine whether rolling in dynamic strain aging conditions improves the texture of the steel when compared to cold rolling. Characterization of the shear bands formed during cold rolling and rolling in dynamic strain aging conditions would also improve the conclusions of this

study. Finally, the effect of bake hardening between 170 and 200°C on the mechanical properties of the steel should be investigated. A good understanding of the effect of bake hardening (thermal cycles necessitated by painting procedures) will be needed to assess the viability of using CASTRIP steel in the automotive industry.

5. CONCLUSION

This study shows four different thermomechanical processing routes to produce dual phase steel that meets ASTM A1079 DP 980 mechanical property standards from CASTRIP hot band. The first process that met DP 980 standards was cold rolling to a 65% reduction and isothermally heat treating. The second process was continuously annealing CASTRIP hot band at an intercritical temperature of 760°C. The third and fourth process began with batch annealing the CASTRIP hot band at 649°C for 48 hours to grow carbides throughout the microstructure. After batch annealing, the steel was cold or warm rolled to a 20% reduction and continuously annealed at an intercritical temperature of 810°C.

CASTRIP is limited to a 20% reduction, which limits the texture improvement that can be achieved by cold rolling. To improve the texture of the steel, rolling in dynamic strain aging conditions was investigated. Tensile properties and XRD pole figure results did not show a significant difference between the warm rolled steel, and the CASTRIP hot band. However, Vickers hardness tests and differential scanning calorimetry tests did show that the warm rolling steel resulted in more work than the cold rolling steel. Based upon the XRD pole figure results, it appears that warm rolling did not rotate the grains further than cold rolling. A conclusive study on whether warm rolling at low to medium reductions rotates grains further than cold rolling is a topic for additional research.

BIBLIOGRAPHY

[1] D.T. Llewellyn and R. Hudd, Steels: Metallurgy and Applications, 3rd Edition, Butterworth Heinemann, 2004

[2] ASTM A1008/A1008M-18 Standard Specification for Steel, Sheet, Cold-Rolled, Carbon, Structural, High-Strength Low-Alloy, High-Strength Low-Alloy with Improved Formability, Solution Hardened, and Bake Hardenable, ASTM International, West Conshohocken, PA, 2018, https://doi.org/10.1520/A1008_A1008M-18

[3] United States Steel Corporation, Extra Deep-Drawing Steel (EDDS), January 28th, 2016, www.ussteel.com

[4] ASTM A568/A568M-17a Standard Specification for Steel, Sheet, Carbon, Structural, and High-Strength, Low-Alloy, Hot-Rolled and Cold-Rolled, General Requirements for, ASTM International, West Conshohocken, PA, 2017, https://doi.org/10.1520/A0568_A0568M-17A

[5] D.T. Llewellyn, Steels Metallurgy and Applications, 2nd Edition, Butterworth-Heinemann, Ltd, Oxford, UK, 1992

[6] P. Ghosh and R.K. Ray, Automotive Steels, Design, Metallurgy, Processing and Applications, Woodhead Publishing, 2017, Chap. 5, Deep Drawable Steels, pg. 113-141

[7] L.J. Ruiz-Aparicio, C.I. Garcia, and A.J. DeArdo, Development of {111} Transformation Texture in Interstitial-Free Steels, Metallurgical and Materials Transactions A, Volume 32A, 2001, pg. 2325-2334

[8] L.J. Ruiz-Aparicio et al, Proceedings of IF Steels, Warrandale, PA, USA, 2000, ISS, 85

[9] B.L. Bramfitt and P.C. Mangonon, Jr, Metallurgy of Continuous-Annealed Sheet Steel, TMS-AIME, Warrendale, PA, 1982

[10] Technology of Continuously Annealed Cold-Rolled Sheet Steel, Pradhan, Ed., TMS, Warrendale, PA, 1985

[11] R. Pradhan, Metallurgy of Vacuum-Degassed Steel, TMS, Warrendale, PA, 1990

[12] T.C. Hsu and S.Y. Lee, A Definition of Drawability and its Relation to Deformation in the Drawing of Square Cups, Journal of Testing and Evaluation, JTEVA, Vol. 4, No. 5, 1976, pp. 340-346

[13] W.T. Lankford, S.C. Snyder, and J.A. Bauscher, New Criteria for Predicting the Press Performance of Deep Drawing Sheets Trans ASM 1950; 42: 1197-1205

[14] H. Tokunaga, Tamada, US patent 4.504,326

[15] L. Meyer, W. Bleck, and W. Muschenborn, Product-Oriented IF-Steel Design, Proceedings of International Forum for Physical Metallurgy of IF Steels, ISIJ, Tokyo, Japan, 1994, pg. 203-222

[16] W.B. Huchinson, K.I. Nilson, and J. Hirsch, Metallurgy of Vacuum Degassed Steel Products, TMS, Warrendale, PA, 1990, pg. 109-126

[17] M. Fukuda, The Effect of Carbon Content against r-value – Cold-Reduction Relations in Steel, Tetsu to Hagane, Vol. 53, 1967, pg. 559-561

[18] G. Kruass, Steels Processing, Structure, and Performance, 2nd Edition, ASM International, 2015, pg. 241

[19] R.K. Ray, Cold Rolling and Annealing Textures in Low Carbon and Extra Low Carbon Steels, International Materials Reviews, 1994, Vol. 39, No. 4, pg. 129-172

[20] L.A.I. Kestens and H. Pirgazi, Texture Formation in Metal Alloys with Cubic Crystal Structures, Materials Science and Technology, 2016, Vol 32, No 13, pg. 1303-1315

[21] W.B. Hutchinson, Development and Control of Annealing Textures in Low-Carbon Steels, International Metals Reviews, 1984, Vol. 29, No. 1

[22] D. Daniel and J.J. Jonas, Measurement and Prediciton of Plastic Anisotropy in Deep-Drawing Steels, Metallurgical Transactions A, Vol. 21, 1990, 331-343

[23] H. Lee, Proceedings of the International Conference on Microstructure and Texture in Steels and Other Materials, Chapter 5, Texture Development in Low Carbon Steels for Automotive Applications, Jamshedpur, India, February 5-7, 2008

[24] D. Rabbe, Simulation of Rolling Textures of B.C.C. Metals Considering Grain Interactions and Crystallographic Interactions and Crystallographic Slip on {110}, {112}, and {123} Planes, Material Science and Engineering A, A197 (1995), 31

[25] H. Inagaki, Formation of {111} Recrystallization Texture in Polycrystalline Iron, Transactions of the Iron and Steel Institute of Japan, Vol. 24, Issue 4, 1984, pg. 266-274

[26] H Inagaki and T. Suda, The Development of Rolling Textures in Low-Carbon Steels, Texture, Volume 1, Issue 2, 1972, 129-140

[27] H. Inagaki, Fundamental Aspect of Texture Formation in Low Carbon Steel, ISIJ International, Vol. 43, No. 4, 1994, pg. 313-321

[28] W.F. Hosford, Mechanical Behavior of Materials Second Edition, Cambridge University Press, 2010, pg. 120

[29] M. Hatherly, G.S. Rohrer, F. Humphreys, A. Rollett, Recrystallization and Related Annealing Phenomena 2nd Edition, Elsevier Science and Technology, 2004, Chapter 2, pg 44-47

[30] M.R. Barnett and J.J. Jonas, Distinctive Aspects of the Physical Metallurgy of Warm Rolling, ISIJ International, Vol. 39, (1999), No. 9, pg. 856-873

[31] M.R. Toroghinejad, A.O. Humphreys, D. Liu, F. Ashrafizadeh, A. Najafizadeh, and J.J. Jonas, Effect of Rolling Temperature on the Deformation and Recrystallized Textures of Warm Rolled Steels, Metallurgical and Materials Transactions A, Volume 34A, May 2003

[32] M. Hatherly, G.S. Rohrer, F. Humphreys, A. Rollett, Recrystallization and Related Annealing Phenomena 2nd Edition, Elsevier Science and Technology, 2004, pg 481

[33] L.J. Ruiz-Aparicio, C.I. Garcia, and A.J. DeArdo, Development of {111} Transformation Texture in Interstitial-Free Steels, Metallurgical and Materials Transactions A, Vol. 32A, 2001, 2325-2334

[34] T. Haratani, W.B. Hutchinson, I.L. Dillamore, and P. Bate, Contribution of Shear Banding to Origin of Goss Texture in Solicon Iron, Journal of Metal Science, Vol. 18, Issue 2, 1984, pp. 57-66

[35] M.C. McGrath, D.C. Van Aken, N.I. Medvedeva, and J. E. Medvedeva, Work Hardening Behavior in Steel with Multiple TRIP Mechanisms, Metallurgical and Materials Transactions A, Vol. 44, 2013

[36] P.Y. Volosevich, V.N. Gridnev, Y.N. Petrov, Carbon Effect on Austenite Stacking Faults Energy in Manganese Steels, Physics of Metals. Metallography, Vol. 40, 1975, pg. 90-94

[37] M. Hatherly and A,S. Malin, Shear Bands in Deformed Metals, Scripta Metallurgica, Vol. 18, 1984, pg. 449-545

[38] World Auto Steel, Steel Eliminates the Weight Gap with Aluminum for Car Bodies, www.worldautosteel.org

[39] World Steel Association, Sustainability Indicator, www.worldsteel.org, 2012

[40] F. Field, R. Kirchain, and R. Roth, Process Cost Modeling: Strategic Engineering and Economic Evaluation of Materials Technologies, JOM, October 2007, pg. 21-32

[41] X. Sun, Failure Mechanisms of Advanced Welding Processes, Chapter 2, Resistance Spot Weld Failure Mode and Weld Performance for Aluminum Alloys, Woodhead Publishing Limited, 2010

[42] D. Spinella, Common Methods Used in Aluminum Structures, Alcoa Technical Center, November 21, 2013, www.alcoainnovation.com

[43] Uddeholm Tooling and SSAB Swedish Steel, Tooling Solutions for Advanced High Strength Steels, presented at Uddeholm Swedish Rally, 2005

[44] M.Y. Demeri, Advanced High-Strength Steels –Science, Technology and Application, ASM International, 2013, pg. 95

[45] J. Huetter, 2015 Nissan Murano bigger, but 145 pounds lighter thanks to high-strength steels, 2015, www.repairerdrivennews.com

[46] G.R. Speich, Fundamentals of Dual-Phase Steels, AIME, 1981, pg. 3-46

[47] N. M. Fonstein et al., Factors that Determine the Level of the Yield Strength and the Return of the Yield-Point Elongation in Low-Alloy Ferrite-Martensite Steels, The Physics of Metals and Metallography, Vol. 104 No. 3, pg. 328-336

[48] J. Zrnik et al., Recent progress in high strength low carbon steels, Comtes FHT, Ltd., Plzen, Czech Republic, ISSN 0543-5846, METABK 45 (4) 323–331 (2006)

[49] N. M. Fonstein, M. Kapustin, N. Pottore, I. Gupta, and O. Yakubovsky, Automotive Steels, Chapter 7 - Dual-phase steels, Editor: Ed. Rana and Singh,, Woodhead Publishing, 2017, pg. 169-216

[50] S. Majumdar, S. Roy, and K.K. Ray, Fatigue Performance of Dual-Phase Steels for Automotive Wheel Application, Fatigue and Fracture of Engineering Materials and Structures, 2016, 1-18

[51] S. Sriram, J.S. Cintamani, and R.S. Bhatnagar, P. Nagle, G. Dobieralski and W. M. Riley, Application of Dual-Phase Steels for Automotive Closure Panels, SAE International Technical Paper Series, 2003

[52] J. Reed, Advanced High-Strength Steel Technologies in the 2015 Ford Edge, Great Designs in Steel, Livonia MI, 13 May 2015

[53] ASTM A1079-17, Standard Specification for Steel Sheet, Complex Phase (CP), Dual Phase (DP) and Transformation Induced Plasticity (TRIP), Zinc-Coated (Galvanized) or Zinc-Iron Alloy-Coated (Galvannealed) by the Hot-Dip Process, ASTM International, West Conshohocken, PA, 2017, www.astm.org

[54] N. M. Fonstein, Advanced High Strength Sheet Steels, Physical Metallurgy, Design, Processing, and Properties, Springer, 2015, Chapter 4, pg. 110, 140 – 177

[55] W. Bleck and K. Phiu-On, Microalloying for Cold-Formable Multi-Phase Steel Grades, Material Science Forum, Vol. 500-501, 2005, pg. 97-112

[56] B. Bayramin, C. Simsir, M. Efe, Dynamic Strain Aging in DP steels at forming relevant strain rates and temperatures, Material Science and Engineering A Vol. 704, 2017, pg. 164-172

[57] T. Obara, S. Satoh, N. Nishida, and T. Irie, Control of Steel Chemistry for Producing Deep Drawing Cold Rolled Steel Sheets by Continuous Annealing, Scandinavian Journal of Metallurgy, 1984, Vol. 13, pg. 201-213

[58] H. Abe and S. Satoh, Progress of Continuous Annealing Technology for Cold-Rolled Sheet Steels and Associated Product Development, Kawasaki Steel Technical Report No. 22, 1990, pg. 48-56

[59] M.R. Barnett and L. Kestens, Strengthening the {111} Texture in Steel Sheet by Increasing the Level of Solute Carbon During Cold Rolling, Textures and Microstructures, Vol. 34, 2000, pg 1-22

[60] H. Hu and S.R. Goodman, Effect of Manganese of the Annealing Texture and Strain Ratio of Low-Carbon Steels, Metallurgical Transactions B, Vol. 1, Issue 11, 1970, pg. 3057-3064

[61] N. M. Fonstein, Advanced High Strength Sheet Steels, Physical Metallurgy, Design, Processing, and Properties, Springer, 2015, pg. 54

[62] N. Phoumiphon, R. Othman, and A.B. Ismail, Conventional Cold Rolling and Intercritical Annealing of Plain Low Carbon Steel, IJMPE, 2016, Vol. 4, Issue 1, pg. 146-149

[63] H. Shirasawa, and J.G. Thomson, Effect of Hot Band Microstructure on Strength and Ductility of Cold Rolled Dual Phase Steel, Transactions of the Iron and Steel Institute of Japan, 1987, Vol. 27, Issue 5, pg. 360-365

[64] G.R. Speich and A. Szirmae, Formation of Austenite from Ferrite and Ferrite-Carbide Aggregates, Trans. TMS-AIME, Vol. 245, 1969, pg. 1063-1074

[65] Y. Mazheri, A. Kermanpur, and A. Najafizabeh, Strengthening Mechanisms of Ultrafine Grained Dual Phase Steels Developed by New Thermomechanical Processing, ISIJ International, 2015, Vol. 55, No. 1, pg. 218-226

[66] T. Gladman, Grain Size Control, Old City Publishing Inc., 2004, pg. 99

[67] Y. Granbom, Effect of Process Parameters prior to Annealing on the Formability of Two Cold Rolled Dual Phase Steels, Steel Research International, 2008, Vol. 79, pg. 297-305

[68] P. Chang and A.G. Preban, The Effect of Ferrite Grain Size and Martensite Volume Fraction on the Tensile Properties of Dual Phase Steel, Acta Metall. Vol. 33, No. 5, pg. 897-903, 1985

[69] B.-C. Hwang, T.-Y. Coa, S.Y. Shin, S.-H. Kim, S.-H. Lee, and S.-J. Kim, Effect of Ferrite Grain Size and Martensite Volume Fraction on Dynamic Deformation Behavior of 0.15C-2.0Mn-0.2Si Dual Phase Steels, Materials Science and Technology, 2005, Vol 21, No 8, pg. 967-975

[70] A.A. GORNI, and O.L.G. BRANCHINI, Análise da Evolução do Encruamento de um Aço Bifásico. In: 4° Simpósio de Conformação Mecânica, EPUSP/UNICAMP/ABAL, São Paulo, 1990, pg. 23-42.

[71] A.A. GORNI, and O.L.G. BRANCHINI, Relações Microestrutura-Propriedades Mecânicas em um Aço Bifásico Laminado a Quente. In: 1º Seminário sobre Chapas Metálicas para a Indústria Automobilística, ABM/AEA, São Paulo, 1992, pg. 127-145

[72] E. Ahmad, T. Manzoor, and N. Hussain, Thermomechanical Processing in the Intercritical Region and Tensile Properties of Dual-phase Steel, Material Science and Engineering A, Volume 508 (1-2), 2009, pg. 259–265

[73] A.R. Salehi, S. Serajzadeh, and A.K. Taheri, A Study on the Microstructural Changes in Hot Rolling of Dual-Phase Steels, Journal of Material Science, 2006, Vol. 41, pg. 1917-1925,

[74] C.C. Tasan, M. Diehl, D. Yan, M. Bechtold, F. Roters, L. Schemmann, C. Zheng, N. Peranio, D. Ponge, M. Koyama, K. Tsuzaki, and D. Raabe, An Overview of Dual-Phase Steels: Advances in Microstructure-Oriented Processing and Micromechanically Guided Design, Annual Review of Material Research, 2015, Vol. 45, pg. 391-431

[75] N. M. Fonstein, Advanced High Strength Sheet Steels, Physical Metallurgy, Design, Processing, and Properties, Springer, 2015, pg. 95

[76] T. Shinozaki, Y. Tomota, T. Fukino, and T. Suzuki, Microstructure evolution during reverse transformation of austenite from tempered martensite in low alloy steel, ISIJ International, 2017, Vol. 57, No. 3, pg. 533-539

[77] X. J. He, N. Terao, and A. Berghezan, Influence of Martensite Morphology and Its Dispersion on Mechanical Properties and Fracture Mechanisms of Fe-Mn-C Dual Phase Steels, Metal Science, 1984, Vol. 18, July, pg. 367-373

[78] N. J. Kim and G. Thomas, Effects of Morphology on the Mechanical behavior of a Dual Phase Fe/2Si/0.1C Steel, Metallurgical Transactions A, 1981, Volume 12A, , pg. 483-489

[79] C.A. N. Lanzillotto and F. B. Pickering, Structure-Property Relationships in Dual-Phase Steels, Metal Science, 1982, Vol. 16, pg. 371-382

[80] Andritz Metals, Furnaces for Strip Processing Lines, Carbon Steel, 2014, www.andritz.com

[81] N. M. Fonstein, Advanced High Strength Sheet Steels, Physical Metallurgy, Design, Processing, and Properties, Springer, 2015, pg. 19

[82] C.-F. Kuang, Z.-W., Zheng, G.-T. Zhang, J. Chang, S.-G. Zhang, and B. Liu, Effect of Overaging Temperature on the Microstructure and properties of 600 MPa Cold-Rolled Dual-Phase Steel, International Journal of Minerals, Metallurgy, and Materials, 2016, Vol. 23, Issue 8, pg. 943-948

[83] M Avrami, Kinetics of Phase Change. I. General Theory, Journal of Chemical Physics. 1939, Vol. **7,** No. 12, pg. 1103–1112

[84] M. Avrami, Kinetics of Phase Change. II. Transformation-Time Relations for Random Distribution of Nuclei, Journal of Chemical Physics, 1940, Vol. 8, No. 2, pg. 212–224

[85] M. Avrami, Kinetics of Phase Change. III. Granulation, Phase Change, and Microstructure, Journal of Chemical Physics, 1941, Vol. 9, No. 2, pg. 177–184

[86] M. Asadi Asadabad, M. Goodarzi, and S. Kheirandish, Kinetics of Austenite Formation in Dual Phase Steels, ISIJ International, 2008, Vol. 48, No. 9, pg. 1251-1255

[87] Y. Mazaheri, A. Kermanpur, A. Najafizadeh, and A. Ghatei Kalashami, Kinetics of Ferrite Recrystallization and Austenite Formation during Intercritical Annealing of the Cold-Rolled Ferrite-Martensite Duplex Structures, Metallurgical and Materials Transactions A, 2016, Vol. 47, pg. 1040-1051

[88] G.R. Speich, Formation of Austenite during Intercritical Annealing of Dual-Phase Steels, Metallurgical Transactions A, 1981, pg. 1419-1428

[89] J. G. Speer, D.K. Matlock, B.C. DeCooman, and J.G. Schroth, Comments on "On the definitions of paraequilibrium and orthoequilibrium" by M. Hillert and J. Agren, Scripta Materialia, 50, 697-9 (2004), Scripta Materialia, 2005, Vol. 52, pg. 83-85

[90] M. Hillert and J. Agren, Reply to comments on "On the definition of paraequilibrium and orthoequilibrium", Scripta Materialia, 2005, Vol. 52, pg. 87-88

[91] F.L.G. Oliveira, M.S. Andrade, and A.B. Cota, Kinetics of Austenite Formation during Continuous Heating in a Low Carbon Steel, Materials Characterization Vol. 58, 2007, pg. 256-261

[92] H. Azizi-Alizamini, M. Militzer, and W. J. Poole, Austenite Formation in Plain Low-Carbon Steels, Metallurgical and Materials Transactions A, 2011, Vol 42, pg. 1544-1557

[93] R.R. Mohanty, O.A. Grinia, and N.M. Fonstein, Effect of Heating Rate on the Austenite Formation in Low-Carbon High-Strength Steels Annealed in the Intercritical Region, Metallurgical and Materials Transactions A, 2011, Vol. 42, pg. 3680-3690

[94] N. M. Fonstein, Advanced High Strength Sheet Steels, Physical Metallurgy, Design, Processing, and Properties, Springer, 2015, pg. 54

[95] J.D. Baird, The Inhomogeneity of plastic deformation (1973) American Society of Metals, Papers Presented at a Seminar of the American Society for Metals Oct. 16 and 17th, 1971 Chapter 8

[96] R.R.U. Queiroz, F.G.G. Cunha, and B.M. Gonzalez, Study of Dynamic Strain Aging in Dual Phase Steel, Material Science and Engineering A, 2012, 543 pg. 84-87

[97] M.S. Shahriary, B. Koohbor, K. Ahadi, A. Ekrami, M. Khakian-Qomi, and T. Izadyar, The effect of dynamic strain aging on room temperature mechanical properties of high MA DP Steel, Material Science and Engineering A, 2012, Vol. 550, pg. 325-332

[98] A.K. Taheri, T.M. Maccagno, and J.J. Jonas, Dynamic Strain Aging and the Wire Drawing of Low Carbon Steel Rods, ISIJ Int. 1995, Vol. 35, No. 12, pg. 1532-1540

[99] M.R. Akbarpour, and A. Ekrami, Effect of Temperature on Flow and Work Hardening Behavior of High Bainite DP Steels, Material Science and Engineering A, 2008, Vol. 475, pg. 293-298

[100] P. Rodriguez, Serrated Plastic Flow, Bulletin of Material Science, 1984, Vol. 6, No. 4, pg. 653-663

[101] Global Steel Report, Global Steel Trade Monitor, U.S. Department of Commerce, International Trade Administration, 2016

[102] S. Ge, M. Isac, and R.I.L. Guthrie, Progress of Strip Casting Technology for Steel; Historical Developments, ISIJ International, 2012, Vol. 52, No. 12, pg. 2109-2122

[103] C. Klinkenberg, B. Kintscher, K. Hoen, and M. Reifferscheid, More than 25 Years of Experience in Thin Slab Casting and Rolling Current State of the Art and Future Developments, Steel Research International, 2017, Vol. 88, No. 10

[104] A. Chatterjee and S. Chandra, Thin-slab Casting – New Possibilities, Sadhana, 2001, Vol. 26, pg. 163-178

[105] A. Maleki, A. Taherizadeh, and N. Hosseini, Twin Roll Casting of Steels: An Overview, ISIJ International, 2017, Vol. 57, pg. 1-14

[106] D.J. Sosinsky, P. Campbell, R. Mahapatra, W. Blejde, and F. Fisher, The CASTRIP® Process – Recent Developments at Nucor Steel's Commercial Strip Casting Plant, Metallurgist, 2008, Vol. 52, No 12

[107] R. Wechsler and P. Campbell, The First Commercial Plant for Carbon Steel Strip Casting at Crawfordsville, Manfred Wolf Symposium, Zurich Switzerland, 2002, pg. 70-79

[108] W. Blejde, R. Mahapatra, and H. Fukase, Recent Developments in Project M – The Joint Development of Low Carbon Steel Strip Casting by BlueScope and IHI, METEC Congress, Dusseldorf, Germany, 1999

[109] P. Campbell, W. Blejde, R. Mahapatra, and R. Wechsler, Recent Progress on Commercialization of Castrip® Direct Strip Casting Technology at Nucor Crawfordsville, Metallurgist, 2004, Vol. 48, No. 10, pg. 39-43

[110] R. Mahapatra, W. Blejde, P. Campbell, R. Wechsler, and G. Gillen, Commercial Production of Thin-Strip by Twin-Roll Strip Casting-CASTRIP Process, TMS 2013 Annual Meeting Supplemental Proceedings

[111] T. Haga, Twin Roll Casters for Aluminum Alloys, Journal of Japan Institute of Light Metals, 2009, Vol. 59, pg. 509-520

[112] A. Girgensohn, A.R. Buchner, and K.H. Tacke, Twin Roll Strip Casting of Low Carbon Steels, Ironmaking and Steelmaking, 2000, Vol. 27, pg. 317-323

[113] M. Ferry, Direct Strip Casting of Metals and Alloys, Woodhead Publishing Limited, Cambridge, England, 2006, Vol. 48, pg. 76-85

[114] R.I.L. Guthrie, M. Isac, J.S. Kim, and R.P. Tavares, Measurements, Simulations, and Analyses of Instantaneous Heat Fluxed from Solidifying Steels to the Surfaces of Twin Roll Casters and of Aluminum to Plasma-Coated Metal Substrates, Metallurgical and Materials Transactions B, 2000, Vol. 31, pg. 1031-1047

[115] R. Mahapatra, W. Blejde, P. Campbell, R. Wechsler, and G. Gillen, The Status of Twin-Roll Strip Casting Technology – Castrip® Process, Scanmet II – 2nd International Conference on Process Development in Iron and Steelmaking, Lulea, Sweden, 2004

[116] C.R Killmore, A. Phillips, H. Kaul, J.G. Williams, H. Creely, P. Campbell, M. Schueren, and W. Blejde, Development of Ultra-Thin Cast Strip Products by the CASTRIP Process, AIST, Indianapolis, USA, 2007, pg. 7-10

[117] G. Krauss, Steels, Processing, Structure, and Performance, 2nd Edition, ASM International, 2015, pg. 244

[118] G.J.K. Harrington, Effect of solid solutions and second phases on the thermal conductivity of zirconium diboride ceramics, Doctoral Dissertations, 2014, pg. 2343

[119] C. Wert and C. Zener, Interstitial Atomic Diffusion Coefficients, Physical Review, 1949, Vol. 76, Issue 8, pg. 1169–1175

[120] C.H. Suh, Y.-C. Jung, and Y.-S. Kim, Effects of thickness and surface roughness on mechanical properties of aluminum sheets, Journal of Mechanical Science and Technology, Volume 24, Issue 10, 2010, pg. 2091-2098

VITA

Brenton Allen Hrebec was born in Oklahoma City and shortly thereafter was moved to Willard, MO, where he grew up and went to high school. He earned a Bachelor of Science in Metallurgical Engineering from Missouri University of Science and Technology in May of 2017. His graduate school career under Dr. David C. Van Aken was from June 2017 to May 2019, and in July 2019 he received his Master of Science in Metallurgical Engineering from Missouri University of Science and Technology.